Counterclockwise rotation of Late Eocene – Oligocene forearc deposits in southern Peru and its significance for oroclinal bending in the Central Andes

Pierrick Roperch, Thierry Sempere, Orlando Macedo, César Arriagada, Michel Fornari, Claudio Tapia, Marcelo Garcia, Carlo Laj

Counterclockwise rotation of late Eocene–Oligocene fore-arc deposits in southern Peru and its significance for oroclinal bending in the central Andes

Pierrick Roperch,[1,2] Thierry Sempere,[3] Orlando Macedo,[4] César Arriagada,[2] Michel Fornari,[5] Claudio Tapia,[2] Marcelo García,[6] and Carlo Laj[7]

Received 6 July 2005; revised 20 February 2006; accepted 14 March 2006; published 1 June 2006.

[1] The results of a paleomagnetic study along the fore arc of southern Peru (15–18°S) and northern Chile (18–19°S) are reported from middle to late Miocene ignimbrites (7 sites), late Oligocene to early Miocene ignimbrites (72 sites), Paleogene sediments (20 sites), and Mesozoic and Paleocene volcanics and intrusions (31 sites). Comparison of locality-mean directions with expected paleomagnetic directions indicates vertical axis rotations ranging from 5.2 ± 11.3° clockwise to 55.6 ± 7.0° counterclockwise. Spatially, the magnitude of counterclockwise rotations increases northward from ~0° within the Chilean fore arc south of 18°30′S to >45° north of 16°30′S. In southern Peru, paleomagnetic rotations recorded in Paleogene red beds decrease from late Eocene to late Oligocene, whereas Miocene ignimbrites display no evidence of rotation. These new results confirm that the rotations recorded in the fore arc of southern Peru were acquired at least before ~15 Ma, and probably before 25 Ma, and thus prior to the late Neogene shortening of the sub-Andes. The onset of major Andean shortening in the Eastern Cordillera during the latest Eocene–earliest Oligocene is interpreted to have triggered the bending of the Peruvian fore arc. The region of the Peruvian fore arc with the largest rotations appears to be the fore-arc counterpart of the Abancay deflection, a remarkable NE-SW offset in the axis of the Eastern Cordillera induced by a major regional preorogenic structure. We underline that the Abancay deflection should be seen as the northwestern boundary, and therefore as a key element, of the Bolivian Orocline. **Citation:** Roperch, P., T. Sempere, O. Macedo, C. Arriagada, M. Fornari, C. Tapia, M. García, and C. Laj (2006), Counterclockwise rotation of late Eocene–Oligocene fore-arc deposits in southern Peru and its significance for oroclinal bending in the central Andes, *Tectonics*, *25*, TC3010, doi:10.1029/2005TC001882.

[1]Institut de Recherche pour le Développement, UR154, and Géosciences Rennes, Université de Rennes 1, Rennes, France.
[2]Departamento de Geología, Universidad de Chile, Santiago, Chile.
[3]Institut de Recherche pour le Développement, Laboratoire des Mécanismes et Transferts en Géologie, Toulouse, France.
[4]Instituto Geofisico del Perú, Oficina Regional de Arequipa, Peru.
[5]Institut de Recherche pour le Développement, Géosciences Azur, Sophia Antipolis, Nice, France.
[6]Servicio Nacional de Geología y Minería, Santiago, Chile.
[7]Laboratoire des Sciences du Climat et l'Environnement, Gif-Sur-Yvette, France.

0278-7407/06/2005TC001882

1. Introduction

[2] During the last two decades, a number of geological and geophysical studies have addressed issues concerning mountain building in the central Andes and especially the Neogene uplift of the Altiplano-Puna plateau. Because the Andes occur where the oceanic Nazca plate is subducted below the continental South American plate, most workers have proposed to relate the building of the Andes and Andean deformation to parameters such as changes in the rate and angle of convergence [*Pardo-Casas and Molnar*, 1987; *Soler and Bonhomme*, 1990], absolute plate motion [*Russo and Silver*, 1994; *Somoza*, 1998], the morphology of the subducting slab [*Sébrier and Soler*, 1991; *Yañez et al.*, 2002] or the subduction of oceanic plateau or aseismic ridges [*Gutscher et al.*, 1999; *Yañez et al.*, 2002]. Most studies attribute the uplift of the Altiplano-Puna plateau to crustal thickening induced by a large amount of shortening as is evident along the eastern side of the Andes [*Lyon-Caen et al.*, 1985; *Isacks*, 1988; *Roeder*, 1988; *Baby et al.*, 1992; *Watts et al.*, 1995]. Estimates of shortening based on allegedly "balanced" cross sections and geophysical data [*Sheffels*, 1990; *Schmitz*, 1994; *Baby et al.*, 1997; *McQuarrie*, 2002; *Müller et al.*, 2002] appear too small to explain the present thickness of the whole Andean chain [*Kley and Monaldi*, 1998]. However, possible lower crustal flow within the central Andes may be important in the mass transfer balance [*Husson and Sempere*, 2003; *Hindle et al.*, 2005; *Gerbault et al.*, 2005]. Models of Andean uplift consider that uplift initiated ~60 Ma ago in the Western Cordillera (WC), developed later and slower within the Eastern Cordillera (EC), and accelerated in both cordilleras starting ~25–20 Ma [*Gregory-Wodzicki*, 2000; *Kennan*, 2000; *Husson and Sempere*, 2003].

[3] The present morphology of the central Andes is characterized by a large bend in the cordillera, referred to as the Bolivian Orocline. *Isacks* [1988] interpreted the along-strike variations in the width of the Altiplano-Puna plateau as due to differential shortening during plateau uplift. A slight original curvature of the Andean continental margin would have been enhanced by differential shorten-

ing during Neogene time, implying rotation of both limbs. Rotations predicted by this model are 5–10° for the southern limb and 10–15° for the northern limb. This tectonic model was supported by early paleomagnetic results obtained mostly along the fore arc [*Heki et al.*, 1983, 1985a, 1985b; *May and Butler*, 1985] (see also review by *Randall* [1998]). However, there is still a significant debate about the timing, spatial variations and even magnitude of rotations [*Macedo-Sánchez et al.*, 1992a, 1992b; *Butler et al.*, 1995; *MacFadden et al.*, 1995; *Randall et al.*, 1996, 2001; *Aubry et al.*, 1996; *Somoza et al.*, 1999; *Somoza and Tomlinson*, 2002; *Coutand et al.*, 1999; *Roperch et al.*, 1999, 2000; *Gilder et al.*, 2003; *Arriagada et al.*, 2000, 2003; *Richards et al.*, 2004; *Rousse et al.*, 2005; *Taylor et al.*, 2005].

[4] In the southern Peruvian fore arc, paleomagnetic data from Mesozoic rocks suggested that counterclockwise rotations are larger than expected from Neogene shortening along the eastern Andes [*Roperch and Carlier*, 1992]. In contrast, *Roperch et al.* [2000] found no evidence for significant rotation in lower Miocene ignimbrites of northernmost Chile; furthermore, the large-volume ignimbrite sheets that cover extensive areas of the fore arc of northernmost Chile and southern Peru display no evidence for deformation induced by a hypothesized Neogene rotation along the fore arc. These observations were interpreted by *Roperch et al.* [2000] as supporting the idea that the large counterclockwise rotations observed in Mesozoic rocks of southern Peru occurred prior to the Neogene. Here we present new paleomagnetic results from Tertiary sedimentary and volcanic rocks from the fore arc of southern Peru and northernmost Chile (Figure 1) in an attempt to better define the amount, distribution, and timing of tectonic rotations in this key area.

2. Geological Setting

2.1. Regional Overview

[5] The central Andes form the largest and most mountainous segment of the Andean Cordillera. This 4000-km-long segment is itself segmented into the northern central Andes (central Peru), Bolivian Orocline (southern Peru, Bolivia, northern Chile, northwestern Argentina), and southern central Andes (central Chile and west–central Argentina). The Bolivian Orocline (BO) is commonly divided into a number of geomorphic zones (Figure 1a), among which the Altiplano plateau is the most characteristic due to its 3600 m mean elevation and >55 km crustal thickness. The Altiplano is bounded by the Eastern Cordillera (EC), which originated mainly from tectonic shortening [e.g., *Sheffels*, 1990], and by the Western Cordillera (WC), where the volcanoes of the subduction arc cluster. Both EC and WC crustal thicknesses are, at least locally, >70 km [*Beck and Zandt*, 2002], but there is no evidence that the WC, unlike the EC, originated mainly from tectonic contraction. The EC appears to have resulted from the Oligocene-Miocene tectonic inversion of a Triassic-Jurassic rift system [*Sempere et al.*, 2002]. East of the EC, between 18°S and 23°S, the Subandean Zone (SAZ), or sub-Andes, is a Neogene fold-and-thrust belt, the foredeep of which underlies the Beni-Chaco lowlands.

[6] Southern Peru is characterized by a number of structural deflections (Figure 1), the clearest being the Abancay deflection [*Marocco*, 1978], where the structural orientation locally becomes as anomalous as NE-SW. Significant strike variations are visible along the sub-Andes of southern Peru. More to the south, the Caravelí deflection is marked by a change in the trend of the Coastal Batholith (CB), which becomes E-W in the Caravelí area (Figure 1b). A deflection is even perceptible in the deep subducting slab (Figure 1a).

2.2. General Structure of the Fore Arc

[7] The fore arc of southern Peru and northernmost Chile displays a somewhat complex structure and geological mapping is currently being revised. Relevant to this paper is the identification of four domains (Figure 1b) identified on the basis of stratigraphic and tectonic characteristics. Figures 1b, 2a, 2b, and 2c highlight the main fault systems here emphasized in southern Peru and northernmost Chile, as well as the distribution of the principal stratigraphic units. The Iquipi Fault (IF) separates the Caravelí and Arequipa domain. The Río Tambo Fault System (RTFS) separates the latter from the Moquegua domain. The Arica domain mainly corresponds to northernmost Chile and is separated from the Moquegua domain by the Río Caplina Fault (RCF).

[8] The Caravelí domain includes a thick Carboniferous to Cretaceous stratigraphic succession that is largely intruded by mostly mid-Cretaceous plutons belonging to the CB. In this domain, the CB strikes approximately E-W, and at Atiquipa crops out on the present coast (Figure 1b). The fore-arc deposits known as the Moquegua Group overlie CB rocks. The Caravelí area corresponds to the inflection point in the Caravelí deflection and is characterized by south verging, E-W reverse faults [*Huamán*, 1985].

[9] The Arequipa domain appears to be nested in the oceanward concave side of the Caravelí deflection. Its entire coastal area is characterized by ~1 Ga old high-grade, granulitic migmatites [*Martignole and Martelat*, 2003] and local Ordovician intrusions [*Loewy et al.*, 2004]. This basement is widely exposed in the southwest and is overlain in the northeast by a thick Upper Paleozoic to mid-Cretaceous succession. In particular, the Upper Jurassic to Paleocene strata include only very minor occurrences of volcanic and volcanodetritic rocks. The CB, which includes Jurassic, Cretaceous and Paleocene plutons, intrudes this succession and crops out along a belt running at the foot of the Western Cordillera, markedly away from the present coastline. Northeast of this belt, the Mesozoic succession has undergone an Andean age shortening [*Vicente*, 1989] of an intensity and style unknown in the other domains. In the Arequipa domain, the Moquegua Group unconformably overlies Mesozoic strata in the northeast, and Precambrian to Paleozoic rocks in the southwest.

[10] The Moquegua domain contrasts with the Arequipa domain on many aspects. Exposures of metamorphic basement display at most amphibolite grade and occur in only 3 small areas (1 on the coast, 2 in the Western Cordillera

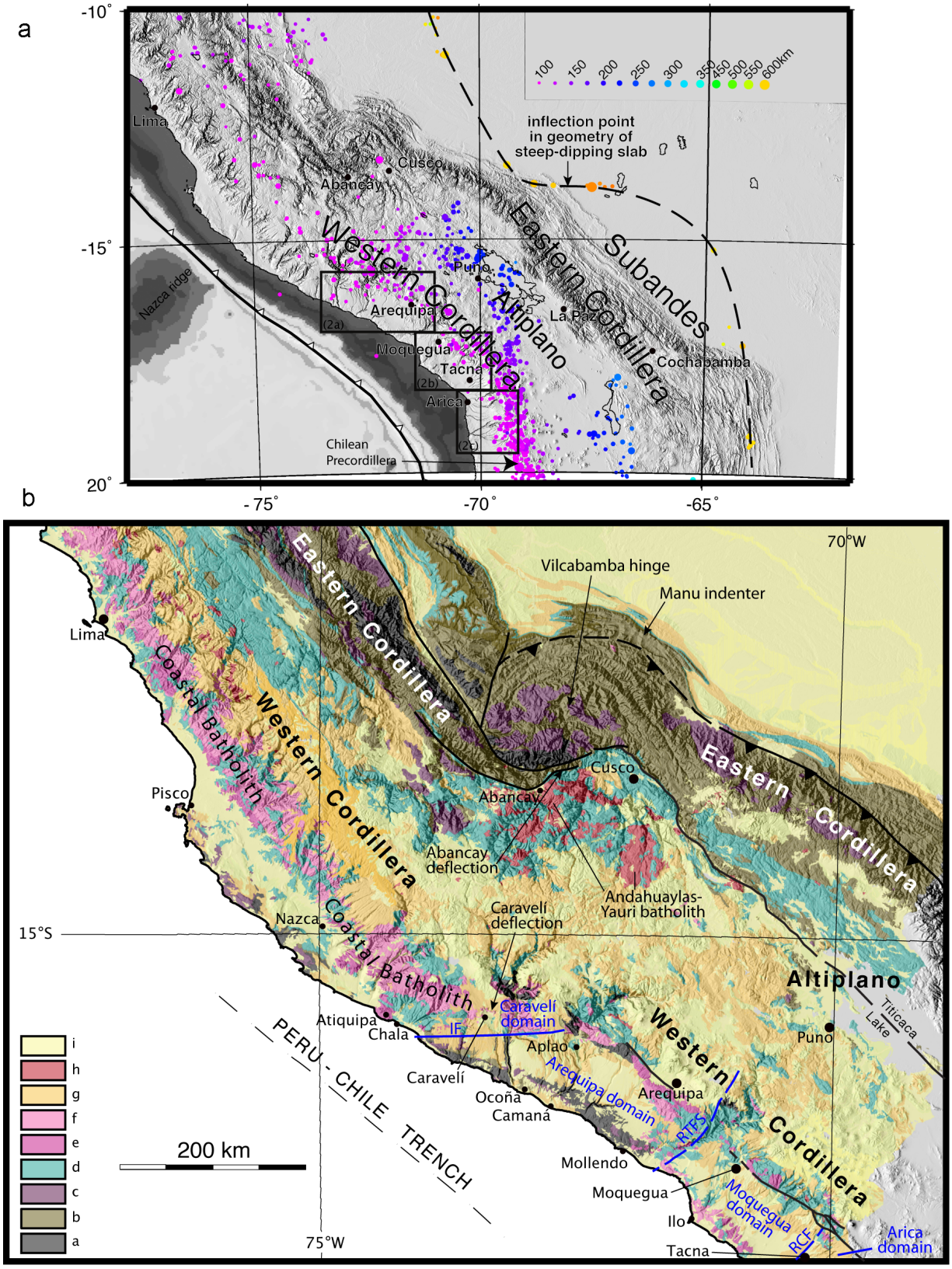
a
-10°
-15°
20°
-75°
-70°
-65°
100
150
200
250
300
350
450
500
550
600km
inflection point
in geometry of
steep-dipping slab
Lima
Cusco
Abancay
Western Cordillera
Altiplano
Eastern Cordillera
Subandes
Puno
Arequipa
La Paz
Nazca ridge
(2a)
Moquegua
Tacna
(2b)
Cochabamba
Arica
Chilean
Precordillera
(2c)
b
70°W
Vilcabamba hinge
Manu indenter
Lima
Eastern Cordillera
Coastal Batholith
Western Cordillera
Pisco
Cusco
Abancay
Eastern Cordillera
Abancay
deflection
Andahuaylas-
Yauri batholith
Caravelí
deflection
Nazca
15°S
Coastal Batholith
Altiplano
Titicaca
Lake
Caravelí
domain
IF
Atiquipa
Chala
Aplao
Puno
Western
Arequipa domain
PERU - CHILE TRENCH
Caravelí
Ocoña
Camaná
Arequipa
RTFS
Cordillera
Mollendo
Moquegua
Moquegua
domain
RCF
Ilo
Arica
domain
Tacna
75°W
200 km
i
h
g
f
e
d
c
b
a

Figure 1

slope). The CB intrudes a thick Upper Paleozoic to mid-Cretaceous succession as more to the northwest, but crops out along two distinct belts, one running along the coast and including Jurassic and mid-Cretaceous plutons, the other running at the foot of the Western Cordillera and including Late Cretaceous–Paleocene intrusions. Also in contrast with the Arequipa domain, the Upper Jurassic to Paleocene strata in the Moquegua domain consist almost exclusively of volcanic and volcanodetritic rocks, that form the >3 km Toquepala Group (in a broad sense); the Moquegua Group almost exclusively overlies the Toquepala Group.

[11] The Arica domain differs from the Moquegua domain in that the Toquepala Group (or its equivalent) is present apparently only north of 18°30′S. Metamorphic basement only occurs in one small area in the Western Cordillera slope, where it is of low grade and intruded by an Ordovician pluton [*Loewy et al.*, 2004]. Mesozoic rocks occur throughout the Precordillera, Central Depression and Coastal Range. In the Precordillera, the Mesozoic strata form an essentially marine sedimentary series, which consists of conglomerates, calcareous sandstones, salt layers and rhyolitic tuffs; this succession is intruded by Late Cretaceous–Paleocene quartz-monzonites, granodiorites and monzodiorites [*Muñoz and Charrier*, 1996; *García*, 2002] that form a stringer continuing the northeast branch of the south Peruvian CB. Older plutons assignable to the southern continuation of the coastal, southwest branch of the south Peruvian CB form a main belt that runs along the present coast (Figure 2c). The Azapa Formation, the local equivalent of the Moquegua Group, overlies the Toquepala Group in the north and Mesozoic units south of 18°30′S.

[12] In northernmost Chile, the main tectonic feature of the fore arc is the Oxaya Anticline, which is bounded to the west by the Ausipar Fault [*Muñoz and Charrier*, 1996; *García and Hérail*, 2005] (Figure 2c). The Oxaya Anticline (OA) is a major gentle fold that can be followed for 50 km along strike with a half wavelength of 25–30 km. It plunges to the south, into the Pampa Sucuna, where the Oxaya ignimbrites form an extensive west dipping (2–3°) monocline locally affected by very gentle minor folds. To the north, in Sierra Huaylillas, the OA grades into a very gentle anticline, which may be up to 40 km wide. The area where the fold is most marked, uplifted and shortened is located between the Lluta and Azapa valleys. The folding occurred in the middle–late Miocene, essentially between 12 and 10 Ma [*García and Hérail*, 2005]. *Wörner et al.* [2002] interpreted the flexure as a consequence of a large gravitational collapse of the Oxaya block with a large normal fault separating the WC and the fore arc in the Belén region. In contrast, *Muñoz and Charrier* [1996] and *García and Hérail* [2001] suggested that the OA formed as a consequence of the WC overthrusting the fore arc.

[13] In southern Peru, plutons belonging to the CB have yielded ages mostly comprised within the middle Cretaceous–early Eocene interval, but some are older [*Mukasa*, 1986; *Clark et al.*, 1990]. The distribution and ages of volcanic and plutonic rocks suggest that the present-day belt formed by the CB approximately correspond to the position of the coeval subduction arc. In the case of the Moquegua and Arica domains, the existence of two belts separated by ~75 km points to a significant northeastward migration of the arc in the Late Cretaceous. The Coastal Batholith appears as a good marker of large-scale deformation in the southern Peruvian fore arc. As stated above, it concurs to define the Caravelí deflection, to which the Iquipi Fault is intimately associated. A belt of Jurassic and mid-Cretaceous plutons forming a branch of the CB displays an apparent ~60 km dextral offset in the RTFS area (Figure 1b); the Paleocene magmatic belt is however not deflected.

2.3. Stratigraphy of the Cenozoic Fore-Arc Deposits

[14] On the basis of our new $^{40}Ar/^{39}Ar$ geochronological data, and following *Sempere et al.*'s [2004] stratigraphic revision, Eocene to Neogene fore-arc deposits are subdivided into the Moquegua and Camaná groups and their respective subunits.

[15] Exposed strata assigned to the Camaná Group were deposited in fan deltas at the fault-controlled mouths of a few paleorivers (which are all related to present-day rivers); the most significant deposits occur at the mouths of the Camaná, Tambo, Chala-Cháparra and La Planchada (paleo) rivers. In the Camaná fan delta, the Camaná Group consists of two units, informally named "Camaná A" and "Camaná B" that are separated by an erosional unconformity shortly postdated by a tuff dated at 20.8 ± 0.1 Ma (weighted mean of 3 $^{40}Ar/^{39}Ar$ biotite ages [*Sempere et al.*, 2004]). The sediments sampled for paleomagnetism (discussed below) are from the lower part of the Camaná B unit and thus early Miocene.

[16] The Moquegua Group was also deposited in a fore-arc setting, but in a more continental belt running southwest of the WC, diachroneously starting in the Eocene-Oligocene. On the basis of new $^{40}Ar/^{39}Ar$ data (Table 1 and Figure 3) and a revised analysis of the sedimentary record [*Sempere et al.*, 2004] (Figure 4), the Moquegua Group

Figure 1. (a) Grey shaded topography (SRTM 90m) of the central Andes and bathymetry from ETOPO2 data showing the location of the Nazca Ridge. Boxes correspond to the geological maps with paleomagnetic sampling shown in Figures 2a, 2b, and 2c. Color dots correspond to seismicity with depth >100 km. Dot sizes correspond to magnitudes >4.5 (scale with increments of 0.25). The dashed line links the very deep seismicity and shows a sharp deflection beneath northwestern Bolivia. The Peruvian low-angle subduction segment is located north of 14°S and characterized by a gap in intermediate-depth seismicity. (b) Simplified geological map of southern Peru (modified from the 1/1,000,000 digital geological map by INGEMMET). Legend: a, Precambrian rocks; b, Paleozoic strata; c, Paleozoic intrusive rocks; d, Mesozoic sediments and volcanics; e, f, Cretaceous intrusive rocks; g, Tertiary sediments and volcanics; h, Tertiary intrusive rocks; i, Plio-Quaternary cover. IF, Iquipi Fault; RTFS, Río Tambo Fault System; RCF, Río Caplina Fault.

includes four stratigraphic intervals, labeled MoqA through MoqD.

[17] Before ~30 Ma (MoqA + MoqB interval), three separate basins were active, namely the Caravelí-Aplao basin in the west, the Moquegua-Tacna basin in the southeast (these two basins being separated by the Clemesí high), and the small, isolated Jahuay basin northwest of Moquegua (Figure 2b). Fore-arc deposition onlapped and buried the Clemesí high after ~30 Ma, uniting the two larger basins, while the Jahuay basin ceased to be active.

[18] The "Moquegua A" (MoqA) interval is only represented in the western, Caravelí-Aplao basin by ≤250 m of

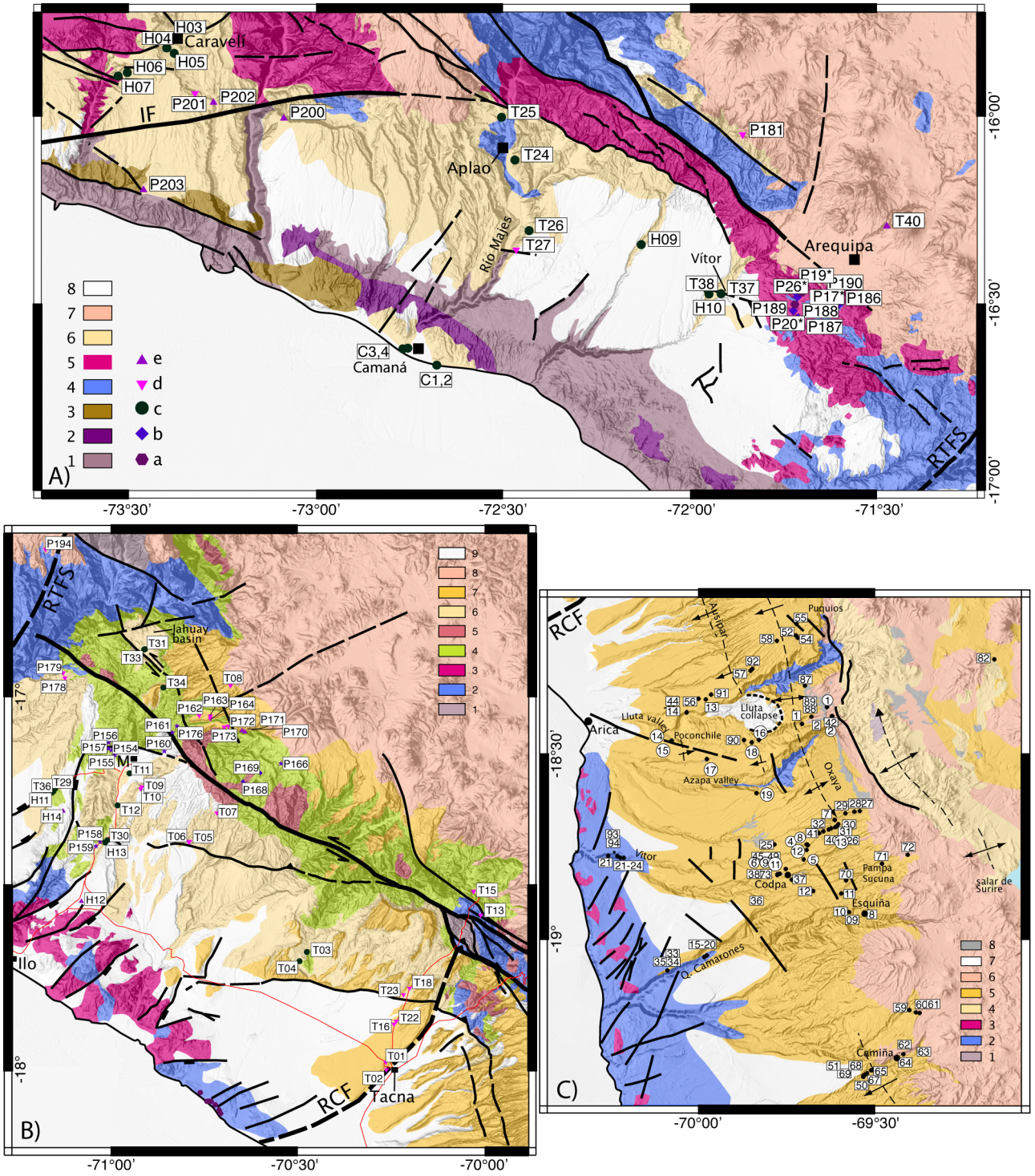

Figure 2

Table 1. Summary of ^{39}Ar-^{40}Ar Results

Sample[a]	Longitude	Latitude	Material[b]	Plateau Age ± 2σ	^{39}Ar, %	n/N[c]	Isochron Age, Ma	Total Gas Age, Ma
				Ignimbrites				
021025-4	−73.415	−15.848	san	9.01 ± 0.07	100	4/4	8.98 ± 0.13	9.11 ± 0.08
021127-T	−71.084	−17.55	biot	9.77 ± 0.12	95	4/7	9.83 ± 0.05	9.68 ± 0.12
011103-3	−72.465	−16.358						
			biot	16.11 ± 0.13	87	8/12	16.12 ± 0.09	15.84 ± 0.16
011104-4	−70.922	−17.249	biot	24.32 ± 0.11	90	6/13	24.72 ± 0.28	24.31 ± 0.12
030801-T	−70.861	−17.113	biot	24.19 ± 0.10	96	5/7	24.14 ± 0.11	24.07 ± 0.10
				Tuffs Within Moquegua Formation				
021024-1	−71.155	−17.254	biot	25.52 ± 0.09	99	8/9	25.46 ± 0.14	25.52 ± 0.14
021024-1			K-Fp	25.53 ± 1.3	100	3/3	26.03 ± 0.64	25.53 ± 1.32
021024-1			amph	25.35 ± 0.30	98	3/4	25.39 ± 1.11	25.45 ± 0.20
011020-1	−70.996	−17.371	biot	29.2 ± 0.82	86	3/4	30.63 ± 0.50	28.07 ± 0.74
011020-1			biot	28.97 ± 1.28	fusion 100	–	28.97 ± 1.28	
011104-2	−71.015	−17.391	biot	31.11 ± 0.54	81	4/5	31.24 ± 1.14	29.42 ± 0.52
011104-2			biot	31.77 ± 0.56	93	3/4	30.70 ± 1.93	31.59 ± 0.54
011104-2			biot	30.71 ± 0.48 31.21 ± 0.32[d]	81	5/8	29.82 ± 1.96	29.05 ± 0.47
021025-5	−73.398	−15.816	amph	43.43 ± 1.84	99	3/4	44.19 ± 1.02	44.34 ± 2.08
021025-5			biot	44.47 ± 0.55	98	4/5	44.30 ± 0.37	44.12 ± 0.58
021025-5			biot	44.45 ± 0.33	98	3/4	44.24 ± 0.22	44.34 ± 0.35

[a]Sample 021025-4 corresponds to ignimbrite V2 of *Huamán* [1985] near Caravelí; 021127-T is paleomagnetic site H12; 011103-3 is paleomagnetic site T27; samples 011104-4 and 030801-T correspond to paleomagnetic site T10; 021024-1 is from a tuff in between site T29 and T35 near Cruz de Portillo; 011020-1 is from volcanic Siltstone with biotites near Cruz del Bronce, a few meters above location of sample 011104-2 and in between sites T30 and H13; 021025-5 is from a volcanic siltstone above site H03 and H04 near Caravelí.
[b]Materials are san, sanidine; biot, biotite; K-Fp, K-feldspar; amph, amphibole.
[c]The plateau age was calculated with n steps out of a total of N steps.
[d]Weighted mean.

red, mostly fine-grained strata devoid of volcanic intercalations. The unit generally overlies plutonic rocks of the CB (Caravelí area, northernmost Río Majes valley, La Joya area), but also Jurassic strata (Río Majes valley) or Precambrian rocks (southern Río Majes valley, and area to the southeast). Near Caravelí, a tuff dated at 44.5 ± 0.4 Ma ($^{40}Ar/^{39}Ar$ on 2 biotites and 1 hornblende) occurs exactly at the MoqA/MoqB boundary. Given the ~250 m thickness of the MoqA unit in this area and its mudstone-dominated lithology [*Marocco*, 1984], an age of ~50 Ma is reasonably estimated for its base. Ages obtained on volcanic rocks of the Toquepala arc in the Moquegua domain are as young 45.9 Ma (hydrothermal alteration [*Clark et al.*, 1990]), and it is likely that deposition of the nonvolcanic MoqA unit in the west was partly coeval with lingering arc activity in the southeast.

[19] The "Moquegua B" (MoqB) interval is represented in all three basins, albeit with somewhat contrasting facies. In the west (Caravelí domain), the MoqB unit mostly consists of coarse conglomerates that overlie the tuff dated

Figure 2. (a) Simplified geological map of the Arequipa region. The paleomagnetic sampling is shown with different symbols: a, sites in Mesozoic rocks from *Roperch and Carlier* [1992]; b, sites in the Late Cretaceous–Paleocene Coastal Batholith (Arequipa area); c, sites sampled in the Moquegua Group; d, sites from late Oligocene–early Miocene ignimbrites; e, sites from late Miocene ignimbrites. Rock units: 1, Precambrian basement; 2, Paleozoic intrusive rocks; 3, Pennsylvanian and older rocks; 4, Permo-Triassic to mid-Cretaceous strata; 5, Late Jurassic–Paleocene intrusive rocks (Coastal Batholith); 6, Moquegua Group and coeval deposits (Eocene-Neogene); 7, Neogene volcanic rocks; 8, late Neogene fore-arc deposits. (b) Simplified geological map of the region (M, city of Moquegua). Rock units: 1, Mississippian and older rocks; 2, Pennsylvanian through Jurassic strata; 3, Late Jurassic and middle Cretaceous plutonic rocks (Coastal Batholith); 4, Late Cretaceous–Paleocene volcanics (Toquepala Group); 5, Late Cretaceous–middle Eocene intrusive rocks; 6, Moquegua Group; 7, Huaylillas and Magollo formations (latest Oligocene–middle Miocene); 8, late Neogene arc volcanic and volcanodetritic rocks; 9, late Neogene fore-arc deposits. (c) Simplified geological map of the Arica region. Site numbers within circles correspond to results previously published by *Roperch et al.* [2000]. Rock units: 1, Belén metamorphic complex; 2, Jurassic through Cretaceous strata; 3, Late Jurassic and middle Cretaceous plutonic rocks; 4, Sediments and ignimbrites of the Lupica Formation (latest Oligocene–early Miocene); 5, Oxaya ignimbrites and Azapa Formations (latest Oligocene–early Miocene); 6, late Neogene volcanic arc; 7, late Neogene fore-arc deposits; 8, late Pliocene Lauca-Pérez ignimbrite.

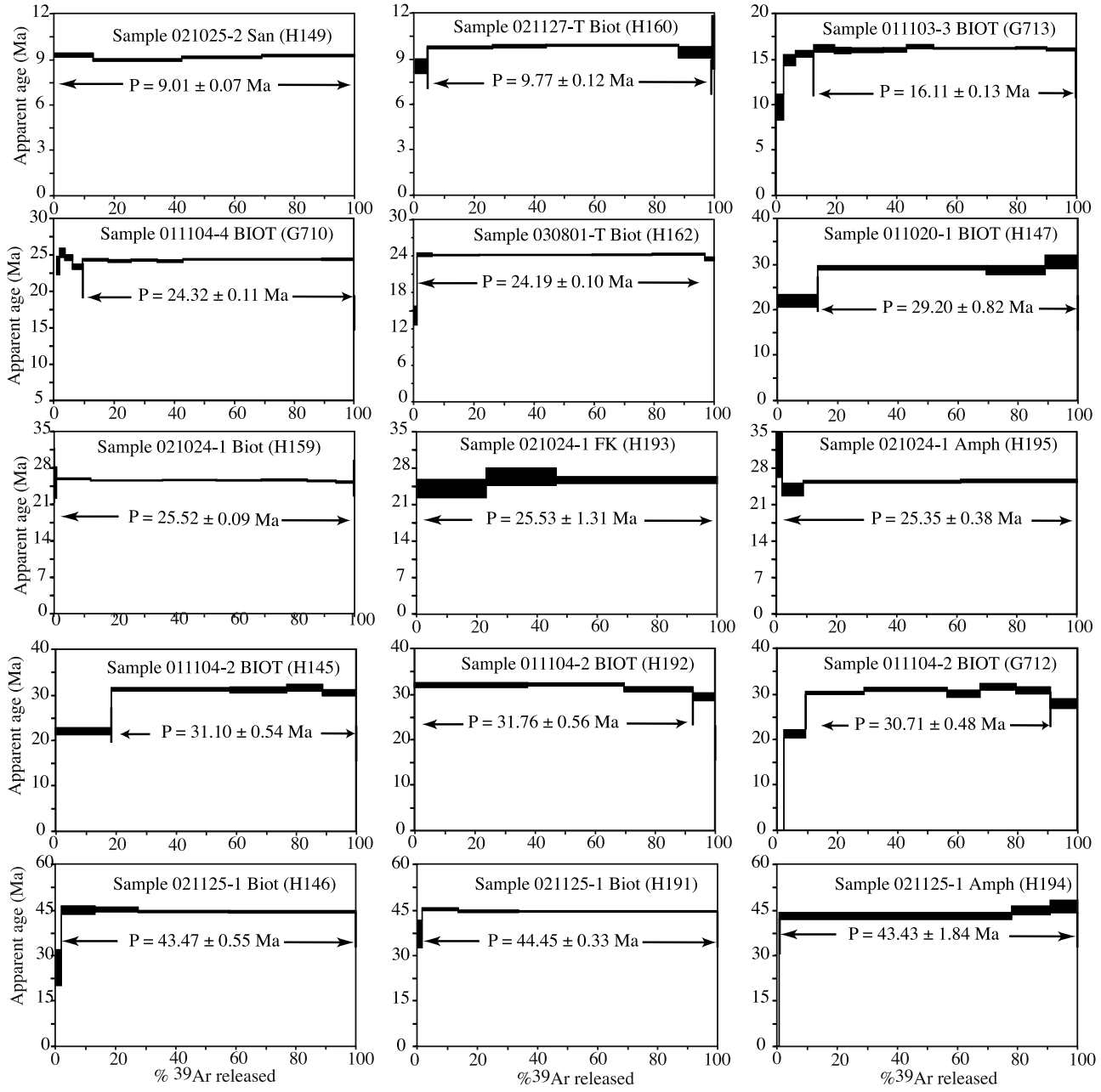

Figure 3. The $^{40}Ar/^{39}Ar$ age spectra of selected samples (Table 1 and auxiliary material). For each step thickness of black rectangles corresponds to 1σ uncertainty on apparent ages, while uncertainties on plateau ages (P) are indicated at the 2σ level.

at 44.5 ± 0.4 Ma. In Aplao (Arequipa domain), conglomerates are also present in the lower part of the unit, but are overlain by dominantly fine-grained red strata. In the Moquegua domain, the MoqB unit mostly consists of fine-grained, locally gypsiferous, red strata and minor aeolian deposits, which onlap volcanic rocks accumulated in the now extinct Toquepala arc. Volcanic material occurs as clasts in the MoqB conglomerates of the Caravelí-Aplao basin, but whether a contemporary lavic volcanism was active is unclear. In all three basins, no explosive volcanic intercalation is known, excepting the basal, ~44.5 Ma tuff in the Caravelí area and a few centimeter-thick tuffaceous levels located only ≤2.5 m below the top of the unit in the Moquegua area, apparently representing precursor events of the abundant explosive volcanism characteristic of the MoqC unit. We have obtained a 31.2 ± 0.3 Ma age on one of these thin levels (see below).

[20] The ~44–31 Ma interval we define for the volcanic-free MoqB unit in the fore arc strikingly coincides with the magmatic activity of the arc defined by the Andahuaylas-

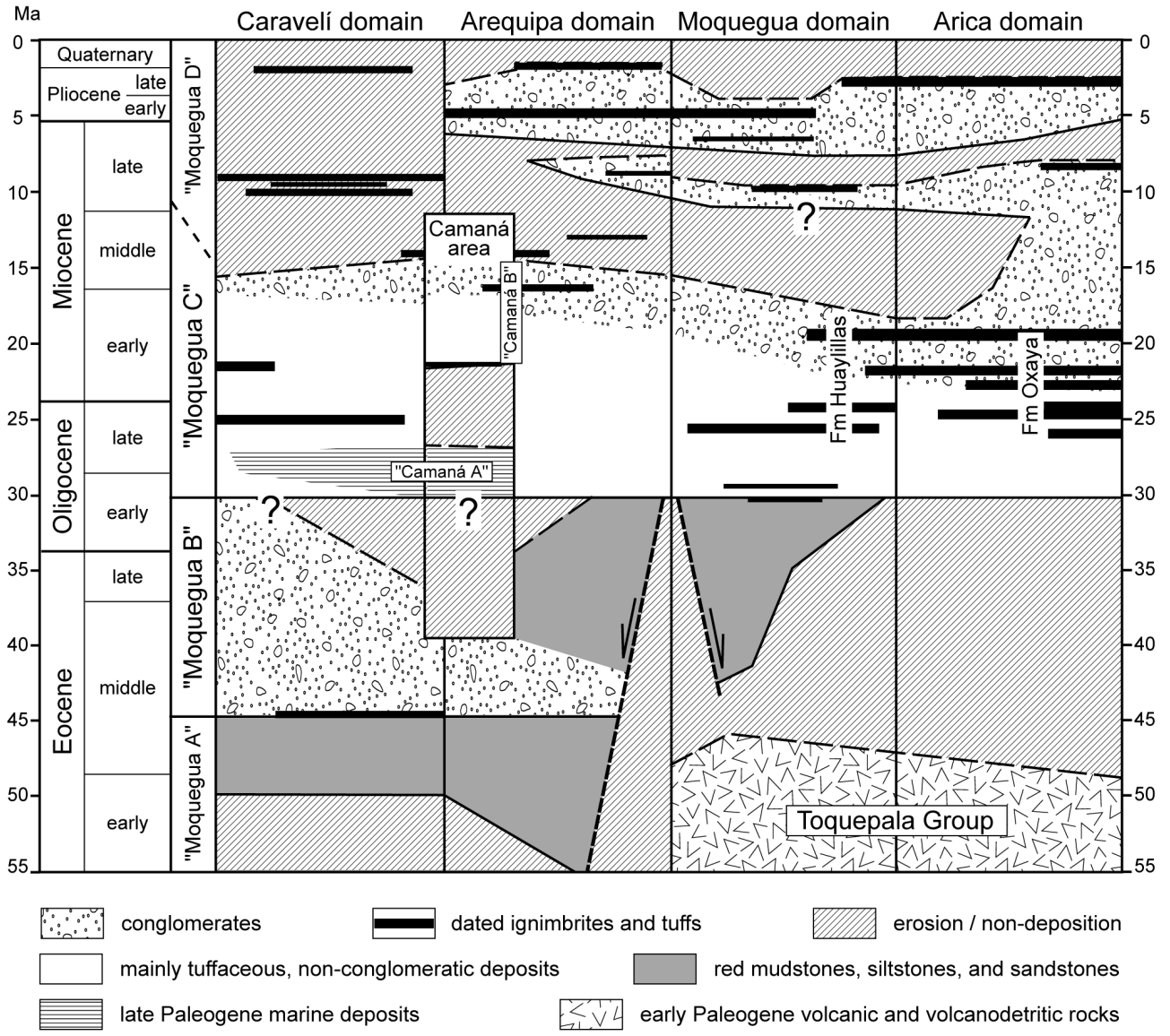

Figure 4. Simplified stratigraphy of the Moquegua Group.

Yauri batholith (Figure 1b). This middle Eocene–early Oligocene (~45–32 Ma) calc-alkaline batholith [*Perelló et al.*, 2003] extends in the highlands south of the Abancay deflection and defines an important porphyry copper province; pluton emplacement, volcanism, and sedimentation are inferred to have accompanied a period of deformation and regional surface uplift. In northern Chile and southern Peru, most of the late Cretaceous–Paleocene magmatism is located to the west of the present-day WC. In southern Peru, however, the Eocene–early Oligocene magmatic belt is clearly offset to the NE when compared to the Paleocene belt, in contrast with northern Chile, where the large Eocene–early Oligocene copper porphyry deposits are located along the eastern edge of the nearby Paleocene arc.

[21] The "Moquegua C" (MoqC) interval is characterized by abundant volcanodetritic material, indicating reactivation of the volcanic arc, now located along the present-day WC. In particular, significant felsic explosive volcanism is reflected by conspicuously abundant tuffaceous material, which confers a general whitish to creamy color to the MoqC unit (in contrast with the dominantly red color of the MoqA and MoqB units, which have therefore been traditionally grouped into a Sotillo or "lower Moquegua" formation). Volcanic relief fed alluvial fans and streams that converged to form the current main rivers, at the mouths of which deltaic sediments accumulated (Camaná B unit); in the continental areas (MoqC unit), deposits consist of sheet and debris flows that rework volcanic material, of some lacustrine sediments, and of pyroclastic beds that locally coalesce to form ignimbritic units (e.g., the Huaylillas Formation). The MoqB/MoqC boundary is generally a lithological to slightly erosional discontinuity. South of Moquegua, we dated tuffs a few meters above and below this discontinuity, which allows us to estimate its age as

~30 Ma (see below). The MoqC interval includes numerous large ignimbrites, many of which have been previously dated by the K/Ar method [*Bellon and Lefèvre*, 1976; *Tosdal et al.*, 1981]. We also report new $^{40}Ar/^{39}Ar$ ages (section 2.4).

[22] The "Moquegua D" (MoqD) interval is characterized by deposition of coarse conglomerates on pediments affecting earlier Moquegua units (Aplao and Arequipa areas) or in deeply incised valleys (Moquegua and Tacna areas). In all areas, the lower boundary of the MoqD unit is markedly erosional. East of Aplao, in a northeastern part of the Arequipa domain, the MoqD conglomerates may even directly overlie MoqA or MoqB strata with a marked angular unconformity. Ignimbrites and tuffs intercalated in the MoqD unit have yielded ages <6 Ma [*Sempere et al.*, 2004], which poorly brackets the MoqC/MoqD discontinuity between ~16 and ~6 Ma; given the observable stratigraphic thicknesses above and below the dated volcanic levels, the MoqC/MoqD boundary is estimated to be diachroneous and ~15–10 Ma in age. In the Moquegua-Tacna region, conglomerates continued to fill valleys until ~2.7 Ma. Erosion has prevailed in all emerged areas since the late Pliocene. The MoqD unit is called Millo Formation west of Arequipa (but has also been referred to as the "upper Moquegua" Formation), Chuntacala Formation in the Moquegua area, and Calientes Formation in the Tacna area. Given its mainly conglomeratic nature, only specific tuffs or ignimbrites could be sampled for paleomagnetic purposes.

[23] The equivalent of the Moquegua Group in northernmost Chile (Arica domain) is the Azapa Formation, which consists of ≤500 m of fluvial conglomerates and sandstones that were deposited over most of the Central Depression, and the eastern part of the Coastal Range. The Azapa Formation onlaps Jurassic–Paleocene rocks in the western Precordillera. The unit is conformably overlain by ignimbrites of the Oxaya Formation *s. l.*, suggesting an Oligocene age for its deposition.

2.4. Large Ignimbrite Deposits in the Fore Arc

[24] The equivalent Huaylillas and Oxaya formations of southern Peru and northernmost Chile, respectively, comprise large and thick rhyolitic ignimbrite sheets that are interbedded with minor fluvial and lacustrine sediments. These units are characteristic of the fore arc east of 71°W. Numerous $^{40}Ar/^{39}Ar$ and K/Ar isotopic datations indicate that the fore-arc ignimbrites were emplaced during the latest Oligocene–early Miocene interval (26.0–19.4 Ma) [*Wörner et al.*, 2000; *García*, 2002; *Farías et al.*, 2005] (Table 1). Their overall thickness is apparently maximum in northernmost Chile, where it reaches 1120 m [*Wörner et al.*, 2000]; it decreases from >500 m in the eastern Precordillera to 0–50 m in the western Central Depression.

[25] In southern Peru, the contact between the MoqC unit and the overlying Huaylillas Formation can be described as transitional due to the fact that ignimbrites are intercalated in the upper part of the MoqC unit and that thin conglomerates are locally intercalated within the coalescent Huaylillas ignimbrites. The oldest $^{40}Ar/^{39}Ar$ age obtained on a >2-m-thick ignimbrite is 25.52 ± 0.09 Ma in the Moquegua area, whereas the youngest $^{40}Ar/^{39}Ar$ age obtained on these ignimbrites is 16.11 ± 0.13 Ma in the Aplao area. Younger (10–9 Ma) and less voluminous ignimbrites are documented in the Peruvian fore arc (Table 1), and sometimes also assigned to the Huaylillas *s. l.* Formation.

3. The $^{40}Ar/^{39}Ar$ Dating

[26] In order to better constrain the age of the Moquegua Group units and paleomagnetic sites, $^{40}Ar/^{39}Ar$ dating was performed on several interbedded tuffs and overlying ignimbrites.

3.1. Sample Preparation and Method

[27] Analyses were performed on individual grains of biotite, amphibole and K-feldspar. The mineral separates were extracted directly from pumice fragments using a microdrill whenever possible; otherwise the rocks were softly crushed then sieved through mesh sizes of 800–500 and 500–300 μm. The powder fractions were cleaned in distilled water in ultrasonic bath and the minerals were selected and handpicked under a binocular microscope. Mineral concentrates were wrapped in aluminum foil and irradiated at the McMaster University's (Hamilton, Canada) nuclear reactor (position 5C) in two batches of 10 and 25 hours. Fish Canyon sanidine was used as a neutron flux monitor (J value determination) assuming an age of 28.02 Ma [*Renne et al.*, 1998]. Ar isotopic concentrations were measured at the UMR Géosciences Azur Laboratory (University of Nice, France). Step heating was performed with a 50-W Synrad CO2 laser. Each step of gas liberation included one minute for heating, followed by two additional minutes of clean up before introducing the gas into the spectrometer. Isotopes were measured in static mode with a VG3600 mass spectrometer using a Daly detector. Blanks for the extraction and purification system, routinely measured every three steps, were in the range of $40–90 \times 10^{-14}$ (^{40}Ar) and $2–10 \times 10^{-14}$ (^{39}Ar) cm^3 STP, and at least 2 orders of magnitude lower than the sample. For ^{36}Ar the blank was $2–3 \times 10^{-14}$ cm^3 STP and near the values measured for the samples. Mass discrimination was monitored by regularly analyzing air pipette volumes. The uncertainty on $^{40}Ar^*/^{39}Ar_K$ of the monitor was estimated at 0.5% and is included in the uncertainty calculation of plateau ages (Table 1). Criteria used to determine plateau ages are that (1) the plateau should contain at least 70% of released ^{39}Ar, (2) the plateau should include at least three consecutive temperature steps, and (3) the integrated age of the plateau should concur within 2σ error of each apparent age from the plateau.

3.2. Results

[28] The isotopic dates obtained in this study are presented in Table 1. Preferred ages correspond to plateau ages. In most samples, the inverse isochron plot of the isotopic ratio produced clusters of points toward the abscissa and, along with the reduced number of steps, resulted in poorly defined regression lines, and thus in isochrons of little

Table 2a. Paleomagnetic Results for Ignimbrites of Southern Peru[a]

Site	Longitude	Latitude	n	D	I	α_{95}	k
Ignimbrites 5–15 Ma							
T40	−71.474	−16.292	9	*187.2*	*58.8*	3.4	229
H12	−71.084	−17.549	6	*7.4*	*−44.2*	2.6	653
P170	−70.647	−17.096	11	*4.9*	*−25.2*	1.5	1119
P171	−70.655	−17.093	11	*357.5*	*−34.9*	2.6	330
P200	−73.086	−16.003	13	179.8	25.4	1.8	557
P202	−73.274	−15.961	10	181.5	25.9	1.7	818
200 + 202				*180.6*	*25.6*		
P203	−73.461	−16.194	14	*0.7*	*−38.2*	2.4	287
Site mean			6	**182.7**	**37.8**	10.8	39
Ignimbrites 25–15 Ma							
T01	−70.270	−17.984	15	*340.9*	*−58.2*	2.1	329
T18	−70.206	−17.787	8	*175.4*	*37.4*	4.9	127
T16	−70.247	−17.882	13	170.3	52.0	1.0	1831
T22	−70.242	−17.875	13	172.4	48.5	2.1	408
Mean 16 + 22				*171.3*	*50.2*		
T23	−70.223	−17.804	10	*180.1*	*50.9*	2.6	340
T05	−70.796	−17.395	11	*22.2*	*−39.0*	3.2	203
T27	−72.464	−16.357	7	214.9	−66.7	4.3	195
Tilt corrected				*2.1*	*−45.3*	4.3	195
P178	−71.128	−16.958	12	4.6	−32.5	3.6	147
P179	−71.133	−16.944	8	7.1	−35.3	5	126
Mean				*5.8*	*−33.9*		
P181	−71.859	−16.050	6	*336.8*	*−43.4*	17.6	21
P185	−71.058	−16.244	10	*168.5*	*54.7*	4	124
P194	−71.180	−16.614	11	*173.4*	*61.2*	7.5	44
P201	−73.323	−15.940	11	*179*	*38.1*	3.5	147
T08	−70.685	−16.977	8/8	203.2	73.3	4.5	150
P162	−70.769	−17.058	10	227.8	75.1	4.9	99
P163	−70.739	−17.059	11	203.5	71.7	5.5	73
P164	−70.739	−17.066	10	209.2	70.9	3.7	168
Mean			4	*210.2*	*73.0*	4.2	469
T07	−70.721	−17.318	12	47.4	71.6	3.5	153
T09	−70.925	−17.253	11	49.8	61.7	5.8	62
P172	−70.691	−17.086	14	61.7	76.0	2.2	341
P173	−70.739	−17.066	10	72.3	75.4	1.8	886
Mean[b]			4	55.8	71.4	8.5	117
Site mean			12	**178.1**	**49.5**	8.0	31

[a]The n is number of samples used in the calculation of the mean direction; D and I are mean declination and inclination in situ and after tilt correction; α_{95} is semiangle of 95% of confidence; k is Fisher's precision parameter. Results in italic are used in the site-mean calculation. Results in bold are the site-mean directions used for tectonic rotations.

[b]This direction is an intermediate direction of the field not used in the

utility. However, isochron age results are concordant with the plateau and total gas ages at the 2σ level (see auxiliary material for analytical data).[1]

[29] Most of the experiments provided spectra (Figure 3) with acceptable age plateau. Some biotite spectra (G713, H147, G712, Figure 3) show progressively increasing apparent ages at low temperature before a main flat segment defining a plateau. This pattern concerns a small amount (<15%) of the total ^{39}Ar degassed and has only a small influence on the calculated ages (concordant plateau, isochron, and total gas ages). It may result from a slight alteration of the analyzed biotites.

[30] In sample 011104-2, which is located ∼2 m below the MoqB/MoqC discontinuity, plagioclase crystals consist of albite and only small biotite crystals were available for dating. The amount of gas released in each step was relatively small. The results from three experiments are concordant at 2σ level and provide a weighted mean age of 31.21 ± 0.32 Ma. This age is ∼2 Myr older than the 29.2 ± 0.8 Ma age obtained on sample 011020-1, which was collected ∼5 m above sample 011104-2 and ∼3 m above the MoqB/MoqC discontinuity. This 29.2 ± 0.8 Ma age is given by a biotite plateau age including three of four steps and representing 86% of the total ^{39}Ar released, and is in agreement with a 29.0 ± 1.3 Ma total fusion age of a smaller biotite crystal. These two ages thus bracket the age of the MoqB/MoqC discontinuity between 31.2 ± 0.3 and 29.2 ± 0.8 Ma. Using these dates and the stratigraphic intervals reported above, we calculate an age estimate of 30.4 ± 0.5 Ma, i.e., ∼30 Ma, for the MoqB/MoqC discontinuity.

4. Paleomagnetic Sampling and Methods

[31] At each site drilled in fine-grained sediments, oriented samples were collected from several beds with cumulative stratigraphic thickness usually between 1 and 10 m. Samples from Tertiary sediments were collected in fine mudstones or siltstones and drilled using air cooling instead of water cooling. In volcanic rocks, each site corresponds to a single cooling unit. Even though ignimbrites have highly stable remanent magnetizations and provide an excellent record of the earth magnetic field, there are several factors that should be taken into account for an application to tectonics. One is that ignimbrites sheets are not numerous enough within a short time interval to fully average secular variation of the geomagnetic field. This is why paleomagnetic results from ignimbrites were averaged in two time windows of 5 and 9 Myr. The second factor is that ignimbrite units are usually geographically widespread but in the field it is not always possible to identify a specific unit at different sites several tens of kilometers apart. When the paleomagnetic or/and field evidences reasonably suggested that the same ignimbrite was sampled at different sites, a mean direction was calculated for the ignimbrite. In addition to the sampling described in this paper (Tables 2a, 3, and 4), we also use here previously unpublished results obtained on Paleogene volcanic rocks and Miocene ignimbrites, that were reported in detail by *Macedo-Sánchez* [1993] (Figures 2a and 2b). Samples were usually oriented with a magnetic compass, and whenever possible with a sun compass.

4.1. Latest Oligocene-Miocene (25–9 Ma) Ignimbrites

[32] Unfortunately, only a few ignimbrites or tuffs are intercalated in the upper MoqC unit and available for sampling. The oldest ignimbrites that yielded paleomagnetic results in Peru are located in the Caravelí area (24.9 ± 0.4 Ma; "V1 ignimbrite" of *Huamán* [1985]) and in the area north of Moquegua (23.7 ± 0.1 Ma). The former was sampled in one site by *Macedo-Sánchez* [1993]. In the Aplao valley, only one ignimbrite (T27), dated at 16.1 Ma, is intercalated in the entire MoqC unit. Site T40 corresponds to an ignimbrite overlying the basement in the Rio Chili valley near Arequipa (∼13.3 Ma [*Paquereau et al.*,

[1]Auxiliary material is available at ftp://ftp.agu.org/apend/tc/2005tc001882.

Table 2b. Paleomagnetic Results for Miocene Ignimbrites of Northern Chile[a]

Site	Longitude	Latitude	n	D	I	α_{95}	k
Sucuna							
AR13	−69.627	−18.704	8	148.1	29.3	2.2	638
C71	−69.484	−18.797	6	139.9	37.1	3.3	423
C72	−69.414	−18.774	11	146.7	33.8	2.3	449
C26	−69.616	−18.700	12	145.8	30.5	1.5	797
C40	−69.634	−18.707	8	145.3	31.1	3.1	316
Mean			5	*145.2*	*32.4*	3.8	399
Oxaya principal unit							
North of Lluta river							
C13	−69.977	−18.357	16	4.8	−24.5	1.6	534
C91	−69.962	−18.345	13	359.6	−19.6	1.6	714
C92	−69.846	−18.277	15	2.0	−24.4	1.8	474
C56	−69.995	−18.355	11	3.4	−25.0	1.6	860
C57	−69.852	−18.281	10	2.9	−28.3	3.2	223
Mean a			*5*	2.5	−24.4	*3.4*	*51*
Pampa Oxaya, east of the flexure							
C27	−69.547	−18.657	10	5.6	−18.3	2.6	366
C28	−69.562	−18.659	9	8.5	−23.8	4.1	157
C29	−69.586	−18.662	8	12.4	−37.2	2.4	534
C30	−69.608	−18.692	10	3.6	−29.4	1.9	668
C31	−69.612	−18.698	9	3.6	−19.4	2.1	579
AR01	−69.637	−18.379	11	9.5	−24.8	1.5	923
C02	−69.641	−18.412	10	5.1	−22.1	1.8	751
C07	−69.616	−18.681	12	357.1	−34.7	3.1	200
C87	−69.699	−18.322	6	9.0	−16.7	2.0	1115
Mean b			9	6.1	−25.2	5.2	*9*
Pampa Oxaya, west of the flexure							
C03	−69.448	−18.187	10	4.2	−34.7	2.5	387
C25	−69.786	−18.745	13	11.1	−23.9	2.9	199
C41	−69.660	−18.715	7	5.6	−29.9	1.6	1482
AR17	−69.973	−18.517	7	6.3	−28.8	2.5	582
AR19	−69.835	−18.608	8	1.1	−25.2	1.8	900
Mean c			5	5.7	−28.5	5.1	*229*
Codpa uppermost unit							
AR05	−69.704	−18.785	11	1.9	−27.7	2.0	502
AR06	−69.756	−18.816	10	0.7	−30.0	2.1	401
AR09	−69.755	−18.813	7	0.1	−27.1	2.8	469
AR10	−69.755	−18.813	9	358.4	−27.6	3.5	216
AR11	−69.753	−18.807	10	2.6	−28.8	1.5	999
AR12	−69.697	−18.760	8	1.2	−29.1	2.4	531
C45	−69.756	−18.814	5	3.9	−31.1	2.2	1242
C46	−69.754	−18.812	5	1.5	−32.4	2.0	1453
C47	−69.753	−18.810	5	3.5	−30.8	2.8	770
C48	−69.752	−18.808	5	2.9	−31.2	2.7	830
C49	−69.755	−18.807	5	5.9	−26.8	2.3	1070
C11	−69.600	−18.877	10	0.2	−29.4	1.6	884
C12	−69.678	−18.870	7	1.7	−23.4	1.8	1080
C37	−69.738	−18.839	8	6.9	−21.8	2.5	505
Mean d			14	2.3	−28.4	1.8	506
Oxaya mean (a + b + c + d)			4	*4.1*	*−26.6*	3.2	838
Oxaya lowermost unit							
AR02	−69.624	−18.403	13	359.9	−38.0	3.0	198
C42	−69.622	−18.402	6	357.0	−37.2	1.2	2925
AR04	−69.695	−18.745	15	2.7	−39.6	1.0	1562
Mean			3	*359.8*	*−38.3*	3.9	1011
Codpa lowermost							
C38	−69.779	−18.827	7	1.5	−14.0	3.0	418
C73	−69.777	−18.825	7	1.8	−17.9	1.5	1555
Mean			2	*1.6*	*−16.0*	-	-
Oxaya							
Coastal area							
C33	−70.088	−19.080	11	10.9	−30.2	1.9	601
C34	−70.088	−19.080	13	10.4	−30.6	3.0	197
C93	−70.235	−18.764	8	8.5	−27.5	2.0	781
C94	−70.235	−18.764	8	8.8	−27.3	1.7	1064
Mean			4	*9.6*	*−28.9*	2.3	1602
Cardones west							
C90	−69.869	−18.466	11	173.3	51.5	1.6	859
C44	−70.030	−18.392	4	167.0	43.2	1.6	3363
AR15	−70.072	−18.467	9	168.6	42.2	2.5	442
Mean			3	*169.4*	*45.7*	8.5	212
Molinos							
C01	−69.707	−18.423	8	*181.5*	*39.7*	3.8	212
Poconchile							
AR14	−70.072	−18.466	10	4.6	−22.3	2.2	479
C14	−70.030	−18.392	13	4.7	−16.6	2.1	388
Mean			2	*4.7*	*−19.5*	-	-
Esquina							
C10	−69.577	−18.926	10	*341.3*	*−67.1*	3.1	250
Puquios lower unit							
C52	−69.724	−18.188	10	187.7	44.4	1.9	628
C54	−69.718	−18.194	8	184.4	46.2	3.0	357
C55	−69.721	−18.157	9	187.0	47.0	2.5	425
Mean			3	*186.4*	*45.9*	2.7	2025
Puquios upper unit							
C58	−69.777	−18.202	10	*171.1*	*45.9*	3.3	229
Region of Camiña							
Camiña 1							
C64	−69.427	−19.306	7	*8.7*	*−38.3*	3.1	374
Camiña 2							
C67	−69.517	−19.350	8	*205.5*	*50.5*	1.9	892
Ignimbrite Moquella							
C50	−69.540	−19.367	10	*1.2*	*−31.0*	1.9	662
Ignimbrite Suca							
C51	−69.539	−19.364	5	7.7	−31.6	3.1	629
C68	−69.529	−19.357	10	11.4	−32.3	3.7	172
Mean			**2**	*9.5*	*−32.0*	-	-
Nama							
C60	−69.391	−19.195	11	192.3	28.1	4.8	91
C61	−69.380	−19.196	8	185.2	37.7	6.9	64
Mean			2	*188.9*	*33.0*	-	-
Altiplano							
C82	−69.171	−18.252	8	*4.0*	*−26.3*	3.8	235
Site mean			17	**181.4**	**36.9**	7.1	26
Mean direction[b]			15	184.3	34.7	5.7	46

[a]Same legend as in Table 2a. AR sites were previously reported by *Roperch et al.* [2000].
[b]Mean direction without the Sucuna and Esquina ignimbrite.

2005]). Site H12 was sampled near Ilo in an ignimbrite dated at 9.8 ± 0.1 Ma (Table 1). In the adjacent Tacna and Arica areas, thick and large ignimbrites dated between 22.7 ± 0.2 and 19.4 ± 0.1 Ma [*Wörner et al.*, 2000; *García*, 2002] are coalescent and form respectively the Huaylillas and Oxaya formations; we performed a dispersed sampling in the widespread outcrops of the Huaylillas Formation, without being always able to secure stratigraphic correlations between sites.

[33] *Roperch et al.* [2000] reported paleomagnetic results from early Miocene ignimbrites of the Oxaya Formation in northernmost Chile. Here we report a more detailed sampling of all the ignimbrites units outcropping west of the WC and one site within the Chilean Altiplano. All the sites reported here were collected at places where the ignimbrites are subhorizontal.

4.2. Eocene-Oligocene (50–25 Ma) Sedimentary Deposits

4.2.1. Moquegua Group and Azapa Formation

[34] Near Caravelí, two sites were sampled in red fine mudstones (H03 and H04) and one site was drilled in red siltstones (H05). Site H07 was drilled in red siltstones above the erosional unconformity between Mesozoic plutonic rocks and the Moquegua Group in Quebrada Corral de Peña. These sites were all drilled in the MoqA unit.

[35] In the Aplao Valley, two sites (T24, T25) were drilled in the bottom part of the MoqA unit near Huancarqui, whereas site T26 was drilled in the lower part of the MoqC unit about 200 m below the mid-Miocene ignimbrite dated at 16.1 Ma (Infiernillo locality). This ignimbrite was sampled farther south, right in the Torán flexure, which deforms the MoqC unit and, to a lesser degree, the MoqD unit (site T27).

[36] Three sites (T37, 38 and H10) were drilled in red mudstones and siltstones belonging to the MoqA or MoqB units along the Panamerican highway at Vítor. Site H09 was drilled at Siguas, also along the Panamerican highway, in coarse sandy sheet flows intercalated in the MoqC unit.

[37] The Paleogene red beds are best observed in the Moquegua region where bedding attitudes vary from subhorizontal to gently tilted. Sites were sampled across the entire succession in several areas (at altitudes varying from ~1000 m up to ~2500 m), but at this stage it is not possible to elaborate a precise composite stratigraphic section including the collected sites. However, sites T11 and T12 correspond to the lowest levels of the Moquegua Group available for sampling in this area, namely the upper part of the MoqB unit. Sites H13 and T30 were collected in brown mudstones at Cruz del Bronce, ~23 km SSW of Moquegua along the Panamerican highway, in the uppermost part of the MoqB unit, ~2 m below the MoqB/MoqC discontinuity here dated at ~30 Ma. Sites T29, T35 and T36 were collected in the MoqC unit at Cruz del Portillo, ~25 km WSW of Moquegua along the Panamerican highway, close to an ignimbritic tuff we dated at 25.5 ± 0.01 Ma (sample 021024-1).

[38] The small Jahuay basin is located ~40 km north of Moquegua at an elevation of ~2500 m and is filled with red beds that unconformably overlie Late Cretaceous–Paleocene volcanics of the Toquepala Group. Two sites (T31 and T33) were collected in the lowermost section of its infill, in well-bedded red mudstones that strongly resemble those known in the MoqB unit outcrops of the Moquegua area in a similar stratigraphic position.

[39] Further southeast, in the Sama valley, sites T03 and T04 were sampled near Canuto in red beds of the MoqB unit, lithologically similar to those near Moquegua.

[40] In contrast with the thick deposits of the Moquegua Group in Peru, outcrops of fine-grained Tertiary sediments are scarce south of Arica. Overall lithologies in the Azapa red beds are similar to those in the Moquegua Group. The sedimentary succession is well exposed at Quebrada Camarones, where the Azapa strata fill a paleotopography caved in the Mesozoic coastal rocks. The only site in the Azapa Formation (C35) corresponds to several red fine-grained beds drilled along the Panamerican highway. The sampling was not distributed continuously but mostly consisted of two groups of samples separated by a vertical gap of a few tens of meters. The uppermost samples at site C35 were collected a few meters below an early Miocene composite ignimbrite consisting of two differently colored units (sites C33 and C34).

4.2.2. Camaná Group

[41] Lower Miocene fine-grained marine sediments (CamB unit) crop out along the coast near Camaná. At each of the four studied sites, several beds were sampled. Site Ca01 and Ca02, located southeast of Camaná, are vertically ~10 m apart. Sites Ca03 and Ca04 were sampled a few kilometers northwest of Camaná in levels that are approximately stratigraphically equivalent to sites Ca01 and Ca02

4.3. Paleocene and Mesozoic Units

[42] East of Camiña, two sites were drilled in Late Cretaceous–Paleocene volcaniclastic sandstones underlying a Neogene succession of ignimbrites and conglomerates. Near Esquiña (site C08), a single Paleocene dike was sampled.

[43] Although several studies have reported paleomagnetic results from Mesozoic rocks in the Arica region [*Heki et al.*, 1985a; *Palmer et al.*, 1980; *Scanlan and Turner*, 1992], the lack of detailed thermal demagnetization makes it very difficult to assess the reliability of these results. Therefore we collected samples also from Cretaceous and Jurassic rocks in order to better constrain the evolution of tectonic rotations in this area. Two sites were drilled in volcanic rocks of the Jurassic Camaraca Formation, six sites in Cretaceous andesitic lavas of the Suca Formation at Quebrada Camarones, one site in sandstones of the Atajaña Formation, and one site in a dike intruding the Atajaña sandstones (Figure 2c).

[44] The Camaraca Formation is a ~4000-m-thick succession of alternating volcanic and marine sediments of Middle Jurassic age, which is intruded by granodiorites of Late Jurassic–Early Cretaceous age (164–143 Ma) [*García*, 2002]. The Atajaña Formation [*Cecioni and Garcia*, 1960] unconformably overlies the Camaraca Formation and consists of sandstones and conglomerates of continental origin; its thickness is approximately 800 m in the Arica region. The Suca Formation [*Cecioni and Garcia*, 1960] is a 2000-m-thick continental volcanic succession intruded by dikes; K/Ar dating indicated minimum ages of ~85 Ma for the dikes and the upper part of the lava succession [*García*, 2002].

4.4. Methods

[45] Measurements were made at the University of Chile. Samples from sedimentary rocks and Mesozoic volcanics

Table 3. Paleomagnetic Results in Late Paleogene Red Beds[a]

Site	Longitude	Latitude	NRM	K (SI)	Strike/Dip	n/N	N/R	In Situ D	In Situ I	α_{95}	k	Tilt-Corrected D	Tilt-Corrected I
Caravelí MoqA ~45 Ma													
H03	−73.398	−15.816	0.0221	0.00143	0/0	14/14	0/14	114.6	41.8	6.4	41	114.6	41.8
H04	−73.399	−15.816	0.0141	0.0013	0/0	8/8	0/8	124.8	39.5	12.7	20	124.8	39.5
H05	−73.379	−15.830	0.00746	0.000857	325/46	10/12	4/0	340.0	−28.5	9.5	29	312.8	−29.5
H03 + H04 + H05						32/34	4/22	129.3	40.9	6.8	15		
H03 + H04 + H05										5.2	25	**121.4**	**38.3**
Coral Peña MoqA ~45 Ma													
H07	−73.528	−15.891	0.004	0.00108	0/0	14/16	0/14	124.1	44.7	6.3	40	**124.1**	**44.7**
Huancarqui	MoqA	~50Ma											
T24	−72.468	−16.116	0.0048	0.000477	0/0	10/11	10/0	312.5	−24.2	10.2	23	312.5	−24.2
T25	−72.504	−16.001	0.00708	0.000749	0/0	8/13	0/5	136.3	38.1	8.9	43	138.8	48.6
T24 + T25						18/24	10/5	130.9	30.6	5.7	41		
T24 + T25										7.2	26	**131.3**	**35.5**
Infiernillo MoqC ~25 Ma													
T26	−72.430	−16.305	0.00434	0.00109	0/0	13/	2/11	151.6	28.1	5.4	60	**151.6**	**28.1**
Vitor	MoqA/B	~45Ma											
H10	−71.948	−16.473	0.00755	0.00183	0/0	12/18	0/12	124.4	39.1	9.4	22	124.4	39.1
T38	−71.953	−16.461	0.0224	0.00128	64/6	10/14	5/5	136.1	19.6	9.9	25	136.6	16.6
H10 + T38						22/32	5/18	130.0	30.1	7.7	17.3		
H10 + T38										8.1	15.7	**130.3**	**28.5**
Moquegua MoqB ~35 Ma													
T11	−70.955	−17.212	0.0256	0.00456	0/0	5/5	0/5	142.8	35.5	14.0	31	142.8	35.5
T12	−70.987	−17.297	0.0272	0.00365	0/0	11/11	0/11	135.2	33.4	9.4	24	135.2	33.4
T11 + T12						16/16	0/16	137.6	34.1	7.3	27.0	**137.6**	**34.1**
Cruz Portillo	MoqC	~25Ma											
T29	−71.154	−17.253	0.0537	0.00201	0/0	5/5	5/0	330.3	−33.9	17.9	19	330.3	−33.9
T35 + 36	−71.163	−17.263	0.014	0.000926	0/0	13/18	7/6	350.4	−43.0	10.4	17	350.4	−43.0
T29 + 35 + 36						18	12/6	164.3	40.8	9.1	16	**164.3**	**40.8**
Cruz Bronce	MoqB/C	~30											
T30	−71.014	−17.390	0.0427	0.00415	58/9	5/7	5/0	336.4	−33.2	10.4	55	335.7	−24.3
H13	−71.020	−17.396	0.0165	0.00274	43/5	12/17	6/6	161.1	41.0	7.4	36	159.3	36.6
H13 + T30						17/24	11/6	159.6	38.7	5.9	38		
H13 + T30										6.2	34	**158.1**	**32.9**
Canuto MoqB ~40 Ma													
T03	−70.481	−17.689	0.0296	0.00596	146/12	10/10	0/10	141.0	39.9	5.3	85	150.7	40.1
T04	−70.500	−17.714	0.0148	0.00409	240/10	9/9	0/9	141.4	24.8	4.3	146	140.5	34.3
T03 + T04						19/19	19	140.1	32.0	4.4	53		
T03 + T04										3.8	72.8	**144.3**	**36.8**
Jahuay ~MoqB ~40 Ma													
T31	−70.913	−16.879	0.0405	0.00189	0/0	7/8	6/0	327.8	−33.4	13.9	21	327.8	−33.4
T33	−70.916	−16.880	0.0367	0.00191	46/8	15/15	15/0	325.3	−34.5	7.1	30	324.7	−30.6
T31 + T33						22/23	21/0	326.0	−34.2	6.0	28		
T31 + T33										5.7	30	**325.6**	**−31.5**
Azapa Formation (Qda Camarones)													
C35[b]	−70.101	−19.084	0.0116	0.00135	0/0	17/23	8/9	176.9	32.2	8.3	20	176.9	32.2

[a]The n/N are number of samples used in the calculation of the mean direction/number of demagnetized samples; N/R are number of characteristic directions with normal and reverse polarities; n − (N + R) is the number of great circles used in the calculation of the mean direction; D and I are mean declination and inclination in situ and after tilt correction; α_{95} is semiangle of 95% of confidence; k is Fisher's precision parameter. Data in bold are used for tectonic rotations (Table 5).

[b]This direction for the Azapa Formation was combined with the normal and reverse polarity results from *von Rotz et al.* [2005] to provide a new mean direction in Table 5.

were usually stepwise thermally demagnetized in ten to fifteen steps from 50°C to 680°C in an ASC furnace with magnetic field <20 nT in the sample region. At each step, room temperature susceptibility was measured to monitor chemical changes during heating. Remanent magnetizations were measured with a JR5A Agico spinner magnetometers. Some samples from the ignimbrites were also measured with a Molspin magnetometer.

[46] In sediments, results from at least four successive temperatures were analyzed by principal component analysis [*Kirschvink*, 1980] to determine sample ChRM directions.

[47] Usually, at least two samples from each ignimbrite site were thermally demagnetized in 10 to 15 steps. When the natural magnetization was obviously univectorial, the other samples were thermally or AF demagnetized in three to five steps. Only sites with evidence of lightning characterized by strong magnetizations with scattered directions underwent detailed AF demagnetization. Results from at least three successive temperature or AF demagnetization

Table 4. Paleomagnetic Results in Paleocene and Cretaceous Rocks[a]

							In Situ				Tilt-Corrected	
Site	Longitude	Latitude	NRM	K (SI)	Strike/Dip	n/N	D	I	α_{95}	k	D	I
Toquepala Volcanics (Southern Peru)												
P154	−71.004	−17.150	nd	nd	0/0	11/11	328.8	−47.7	2.8	266	328.8	−47.7
P155	−70.995	−17.164	nd	nd	0/0	8/8	149.5	39.6	6.8	68	149.5	39.6
P156	−71.011	−17.130	nd	nd	223/25	12/9	132.2	19.4	4.1	162	131.9	44.4
P157	−71.012	−17.146	nd	nd	290/8	10/10	332.1	−9.9	4.4	121	330.8	−15.2
P158	−71.034	−17.396	nd	nd	0/0	8/6/2	330.3	−38.7	4.7	148	330.3	−38.7
P159	−71.045	−17.407	nd	nd	0/0	8/8	327.2	−45.9	2.4	544	327.2	−45.9
P160	−70.862	−17.153	nd	nd	0/0	10/10	336.6	−26.5	2.7	273	336.6	−26.5
P161	−70.841	−17.103	nd	nd	0/0	12/12	315.7	−45.3	2.3	371	315.7	−45.3
P166	−70.551	−17.186	nd	nd	135/18	11/11	139.9	30.5	4.7	96	149.8	27.4
P176	−70.828	−17.086	nd	nd	0/0	8/8	331.5	−51.5	4.8	133	331.5	−51.5
Mean						10/10	326.3	−35.8	9.1	29		
Mean						10/10			7.8	40	**327.6**	**−38.5**
Arequipa Batholith												
P186	−71.600	−16.500	nd	nd	0/0	7/8	163.6	27.1	6.2	95		
P187	−71.709	−16.541	nd	nd	0/0	11/11	127.8	34.0	2.9	218		
P188	−71.724	−16.519	nd	nd	0/0	9/10	113.7	3.8	10.7	29		
P189	−71.768	−16.527	nd	nd	0/0	10/10	130.2	42.8	5.1	76		
P20[b]	−71.711	−16.538	nd	nd	0/0	8/8	133.5	45.4	5.7	95		
P190	−71.706	−16.471	nd	nd	0/0	8/10	320.6	−53.3	4.5	179		
P17[b]	−71.713	−16.474	nd	nd	0/0	8/9	317.2	−34.9	14.8	15		
P19[b]	−71.713	−16.482	nd	nd	0/0	8/9	283.8	−50.7	2.3	565		
P26[b]	−71.713	−16.474	nd	nd	0/0	7/10	287.2	−46.7	16.7	14		
Mean						9/9	**309.1**	**−39.2**	13.7	15		
Intrusif Yarabamba												
P168	−17.234	−70.652	nd	nd	0/0	10/10	168.3	40.7	9.4	29		
P169	−17.211	−70.606	nd	nd	0/0	6/9	150.7	35	7.4	84		
Esquina–Paleocene Dike (Northern Chile)												
C08	−69.531	−18.933	0.409	0.0188	0/0	10/10	357.6	−57.5	4.2	134	357.6	−57.5
Volcanoclastic Sandstones Ksup-Lower Tertiary												
C62	−69.390	−19.298	0.0234	0.000358	10/1	18/19	181.1	52.0	1.7	395	164.7	48.5
C63	−69.427	−19.307	0.00734	0.00058	0/0	7/8	179.3	50.0	3.3	337	179.3	50.0
C63	−69.427	−19.307	0.00734	0.00058	0/0	6/8	6.5	−27.9	5.9	130	6.5	−27.9
Mean						4/4	**1.7**	**−47.0**	15.2	37		
Mean						4/4			16.3	33	357.8	−46.3
Mesozoic Volcanics (Northern Chile) *Camaraca Volcanics*												
C21	−70.020	−18.773	0.288	0.030	340/30	7/7	155.6	27.3	2.9	449	141.7	22
C22	−70.230	−18.770	0.0214	0.000195	340/33	8/11	357.7	−45.9	1.8	961	*321.8*	*−46.5*
Atajaña Formation Cretaceous (Two Sites)												
C23	−70.219	−18.771	0.0298	0.000213	335/14	15/15	357.2	−36.5	2.2	315	346.5	−40.9
C24	−70.204	−18.780	0.227	0.0186	340/10	6/9	355.4	−31.3	3.0	506	349.2	−33.7
Suca Formation Cretaceous (Six Sites)												
C15	−69.984	−19.044	0.582	0.0127	10/25	9/9	16.1	−44.1	2.5	422	352.2	−42.1
C16	−69.985	−19.045	0.549	0.0185	10/25	10/13	6.7	−42.3	2.6	386	346.1	−36.8
C17	−69.985	−19.045	0.370	0.0415	10/25	7/7	11.1	−36.5	2.5	601	353.3	−33.6
C18	−69.986	−19.045	0.0734	0.00113	10/25	7/9	14.1	−41.6	2.3	80	352.5	−39.2
C19	−69.988	−19.047	0.131	0.00116	10/25	9/9	18.4	−41.0	3.6	222	356.4	−40.4
C20	−69.988	−19.047	0.843	0.00756	10/25	8/10	13.7	−39.1	3.9	202	353.8	−36.9
Mean[c]							8.8	−39.3	5.5	104		
Mean[c]									3.0	353	**351.2**	**−38.0**

[a]The n/N are number of samples used in the calculation of the mean direction/number of studied samples; D and I are mean declination and inclination in situ and after tilt correction; α_{95} is semiangle of 95% of confidence; k is Fisher's precision parameter; nd, not determined. Results in bold are listed in Table 5.

[b]Results previously published by *Roperch and Carlier* [1992].

[c]Mean including the two Atajaña sites and the six sites from the Suca Formation.

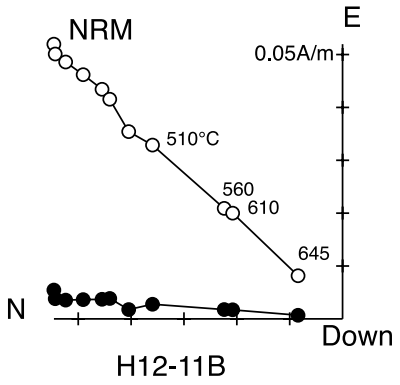

Figure 5. Orthogonal plot of thermal demagnetization of a typical sample in Neogene ignimbrites. The same well-defined ChRM is carried by magnetite and titanohematite. Open (solid) circles are projections onto the vertical (horizontal) plane.

steps were analyzed by principal component analysis [*Kirschvink*, 1980] to determine sample ChRM directions. Because all the demagnetization experiments pointed to a single primary component, all the vectors were anchored to the origin. Maximum angular deviation (MAD) were usually lower than 1°.

[48] Site-mean directions were calculated by applying Fisher statistics [*Fisher*, 1953]. When normal and reversed-polarity directions were present, a single mean direction was calculated by inverting the set of normal directions.

[49] Taking into account that the stratigraphic thickness sampled in sediments varies from a few meters to a few tens of meters, a locality-mean direction was determined using all samples from sites belonging to the same tectonic area and similar stratigraphic ages.

[50] At almost all localities, bedding attitude is nearly horizontal making the application of the fold test either impossible or inconclusive.

[51] The expected direction and tectonic rotations at a paleomagnetic locality were calculated using the appropriate age reference paleomagnetic pole for South America [*Besse and Courtillot*, 2002].

5. Paleomagnetic Results

5.1. Latest Oligocene-Miocene (25–9 Ma) Ignimbrites

[52] Except at a few sites which present evidence of remagnetization by lightning, the ChRMs are well defined and correspond to a thermoremanent or thermochemical magnetization acquired during the emplacement of the ignimbrites (Figure 5). Large variations in magnetic susceptibilities and intensities of remanent magnetizations (Figure 6) are likely to be related to changes in oxygen fugacity prior to or/and during ignimbrite emplacement. Samples with low magnetic susceptibility have unblocking temperatures higher than 580°C and large MDF values showing evidence for highly coercive minerals like hematite and titanohematite. The different magnetic carriers carry the same characteristic magnetization, which supports the hypothesis that the magnetization was acquired upon initial cooling. In most cases, the ChRM was easily identified. In the course of the paleomagnetic study we were able to identify ignimbritic sheets sampled at different sites and showing the same paleomagnetic characteristic direction. Thus using geological and paleomagnetic arguments, paleomagnetic sites with similar directions were grouped together.

5.1.1. Southern Peru: The "Huaylillas" Ignimbrites

[53] In southern Peru, most large ignimbrites have been traditionally assigned to the Huaylillas Formation but geochronological data obtained in the last two decades have shown that individual units are in fact distributed over a large time interval (25–9 Ma). Because of the small number of volcanic units available for sampling, paleomagnetic results from southern Peru have been distributed into two groups according to their isotopic and stratigraphic ages: these groups respectively correspond to middle-late Miocene (14–9 Ma) and latest Oligocene–early Miocene (25–16 Ma) ignimbrites.

5.1.1.1. The 14–9 Ma Ignimbrites of Southern Peru

[54] Normal and reverse magnetizations were observed at sites H12 (9.8 ± 0.1 Ma, northeast of Ilo, Moquegua region) and T40 (13.1 ± 0.1 Ma; ~8 km northeast of Arequipa),

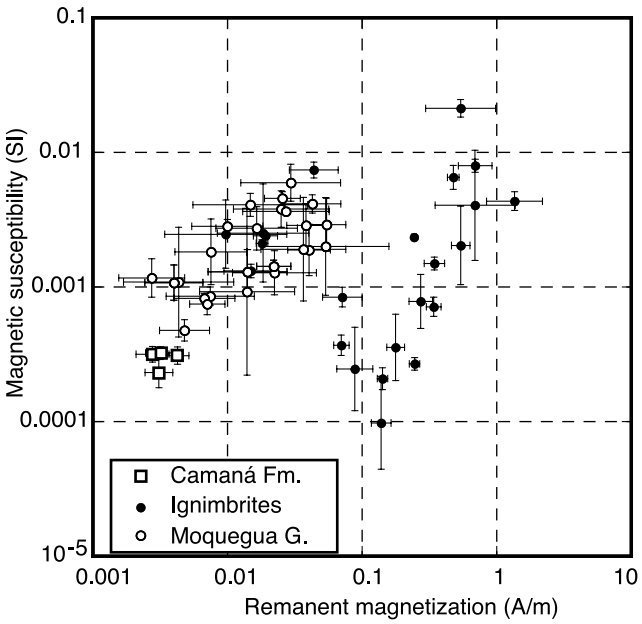

Figure 6. Geometric site-mean intensity of natural remanent magnetization (A/m) versus magnetic susceptibility (SI). Most sites of ignimbrites have thermoremanent or thermochemical magnetization with intensities >0.1 A/m. The Moquegua sediments have high magnetic susceptibilities, indicating a significant amount of detrital magnetite particles. This contrasts with the magnetic characteristics of the Camaná marine sediments showing low magnetic susceptibility and low intensities of NRM.

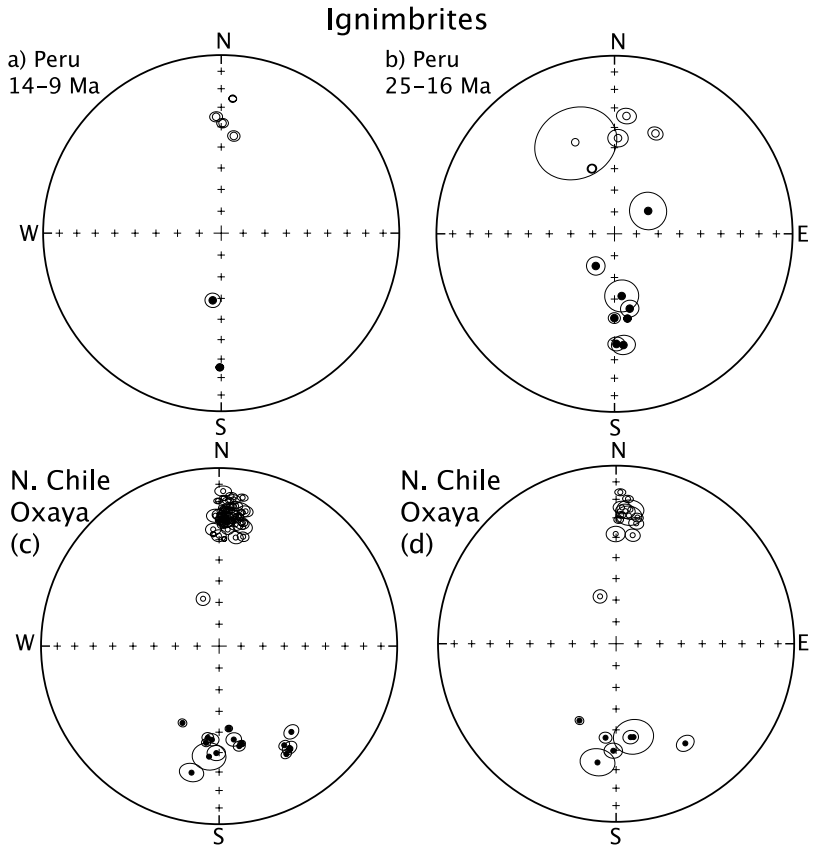

Figure 7. Equal-area plot of the characteristic directions found in ignimbrites. (a) Ignimbrites from southern Peru in the 14–9 Ma interval; (b) ignimbrites from southern Peru in the 25–16 Ma interval; (bottom) site-mean directions in Lower Miocene "Oxaya" ignimbrites; (c) all sites; (d) sites taken within the same ignimbrite sheet were averaged in order to provide independent cooling time units (results listed in Tables 2a and 2b). Open (solid) symbols are projections onto the upper (lower) hemisphere.

respectively. Near Caravelí, two sites (PE200, PE202) were drilled in the "V2 ignimbrite" of *Huamán* [1985], which we dated at 9.0 ± 0.1 Ma (Table 1); their paleomagnetic directions are combined in Table 2a.

[55] Only six different time units are available for this age interval, 4 with normal polarities and 2 with reverse polarities (Figure 7a). The mean direction calculated for these ignimbrites (Table 2a) is close to the expected mid to late Miocene direction.

5.1.1.2. The 25–16 Ma Ignimbrites of Southern Peru

[56] North of Tacna, several sites were sampled in subhorizontal ignimbrites that belong to the Peruvian counterpart of the 24–19 Ma Oxaya Formation. A normal polarity is observed at site T01 whereas the other sites display reverse polarities. Sites T16 and T22 are close to each other in the same unit and their paleomagnetic data were combined to provide a single time unit value.

[57] Farther northwest, near Moquegua, two different ignimbrites with steep inclinations have been identified (Table 2b and Figure 7b). Ignimbrite "Moquegua 1" (sites T07, T09, PE172, PE173), which could not be dated, displays an intermediate direction at >45° from the expected axial dipole field and therefore was not included in the mean calculation. The older, "Moquegua 2", ignimbrite occurs ~40 m below the latter and is dated at 24.3 ± 0.1 Ma. An other ignimbrite belonging to the lower Miocene sequence presents steep inclinations but its characteristic direction is at <45° from the expected direction. Sites drilled in MoqC tuffs ~30 km northwest of Moquegua (P178, P179) have an identical direction and were combined in a single time-cooling unit.

[58] Site T27 was sampled in an ignimbrite dated at 16.1 Ma; it is affected by a steep local flexure ~7 km southwest of Infiernillo and was the only site that needed a tilt correction. Near Caravelí (site PE201), a reverse magnetization was obtained in the "V1 ignimbrite" of *Huamán* [1985], which he dated at 24.9 ± 0.4 Ma. This V1 ignimbrite is the oldest dated unit taken into account here.

[59] The dispersion of the site mean calculated from these 12 independent units is characterized by a Fisher parameter k of 31, indicating that a significant amount of secular variation is averaged. The mean direction calculated for these ignimbrites is not statistically different from that of the 14–9 Ma group and suggests that 25–16 Ma units distributed along the southern Peruvian fore arc did not undergo significant rotations.

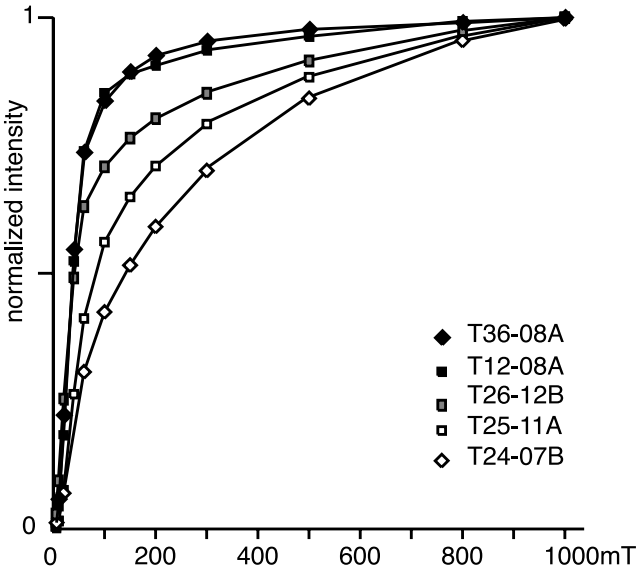

Figure 8. IRM acquisition for five different samples of the Moquegua Group. IRMs show both high coercivities (hematite) and low coercivities (magnetite) magnetic carriers.

5.1.2. Northernmost Chile: The Oxaya Ignimbrites

[60] Paleomagnetic data are numerous (66 sites, Table 2b and Figure 7c) but in many cases several sites correspond to the same ignimbrite sheet. Correlation between sites is however not always straightforward at great distance. Moreover, the area is affected by the Oxaya flexure [*Muñoz and Charrier*, 1996; *Wörner et al.*, 2000]. This is the reason why paleomagnetic results were grouped together within areas where the ignimbrites have the same attitude and where we were clearly able to assert in the field that the paleomagnetic sites belong to the same ignimbrite.

[61] Ignimbrites are rarely deposited on a perfectly flat horizontal surface, and tectonic corrections may be difficult to perform. In an analysis of preliminary results, *Roperch et al.* [2000] assumed a 1.8° down-to-the-west tilting equal to the surface slope. It is however just as likely that the ignimbrites were deposited on an inclined surface.

[62] The most prominent ignimbrite in the Arica region displays a normal polarity and is hereafter referred to as the "main Oxaya unit". This unit has yielded $^{40}Ar/^{39}Ar$ ages on sanidine of 19.4 ± 0.1 Ma [*Wörner et al.*, 2000] and of 19.5 ± 0.1 and 19.7 ± 0.2 Ma [*García*, 2002], providing a mean age of 19.5 ± 0.1 Ma. It crops out on the surface of the Oxaya flexure and can be traced down to the Codpa village as well as up north of the Lluta valley. According to site locations, the results were analyzed over 4 areas (Table 2b): the paleomagnetic directions near Codpa and north of the Lluta valley are nevertheless similar to the directions found east and west of the Oxaya flexure. The four groups of directions are <3° from the mean direction of the Oxaya principal unit. This indicates a lack of paleomagnetically detectable relative rotations or tilt within the Arica region.

[63] At the base of the Oxaya main unit, we found a high inclination (−38.3°) at three sites while near Codpa two sites record a low inclination (−16°). We speculate that these directions may indicate that the base of the thick Oxaya unit is composed of more than one cooling unit. Further work is needed to confirm this hypothesis.

[64] Near Poconchile, two ignimbrites older than the main Oxaya unit are clearly identified on both sides of the Lluta valley. One of them yielded three K-Ar ages on biotite of ∼23.7 Ma [*García*, 2002]. This lowest unit is a <10-m-thick pyroclastic flow, interbedded within horizontal sediments, that records a normal polarity magnetization. Ten to twenty meters above, the Cardones ignimbrite is characterized by a well-developed black vitrophyre and records a reverse polarity; it yielded $^{40}Ar/^{39}Ar$ ages on sanidine of 22.7 ± 0.2 Ma [*Wörner et al.*, 2000] and 21.8 ± 0.3 Ma [*García*, 2002]. Near Puquios, two undated ignimbrites with reverse magnetic polarity are recognized. To the east of the Lluta collapse, we sampled the Molinos ignimbrite, which also records a reverse polarity. Correlations of the Puquios and Molinos with those in the Cardones area are uncertain and we consider that each group records an independent direction.

[65] Above the main Oxaya unit, the Sucuna ignimbrite records a characteristic direction with a southeast declination. This unit has yielded several K/Ar ages on biotites [*García*, 2002], the mean of which, 19.4 ± 0.6 Ma, is undistinguishable from the age of the main Oxaya unit.

[66] The westernmost sites were drilled along the Panamerican highway in a composite ignimbrite showing contrasting white and pink units. These white and pink units record the same paleomagnetic direction, which appears to be statistically different from that of the main Oxaya ignimbrite. We speculate that this western ignimbrite may be distinct from the main Oxaya unit.

[67] Other ignimbrites were sampled along the valley to Camiña and near Nama.

[68] In summary, seventeen independent units, 10 of normal polarity and 7 of reverse polarity, are listed in Table 2b and plotted in Figure 7d. The mean direction is (D = 181.4°, I = 36.9°, α_{95} = 7.1°). Removing the Esquiña pyroclastic flow (24.7 ± 0.3 Ma, $^{40}Ar/^{39}Ar$ on sanidine [*García*, 2002]) and the Sucuna ignimbrite, which both record directions ∼30° apart from the mean, does not significantly modify this mean direction.

5.2. Eocene-Oligocene (50–25 Ma) Sedimentary Deposits

5.2.1. Moquegua Group and Azapa Formation

[69] Samples from the Moquegua Group and Azapa Formation have high magnetic susceptibilities and strong remanent magnetizations (Table 3 and Figure 6). IRM acquisition curves indicate that the magnetic carriers correspond to varying amounts of magnetite and hematite (Figure 8). Thermal demagnetization confirms these dual magnetic carriers with unblocking temperatures widely distributed from 150°C up to 680°C (Figure 9). Both magnetic carriers record the same ChRM direction. Alternating field demagnetization demonstrates that the magne-

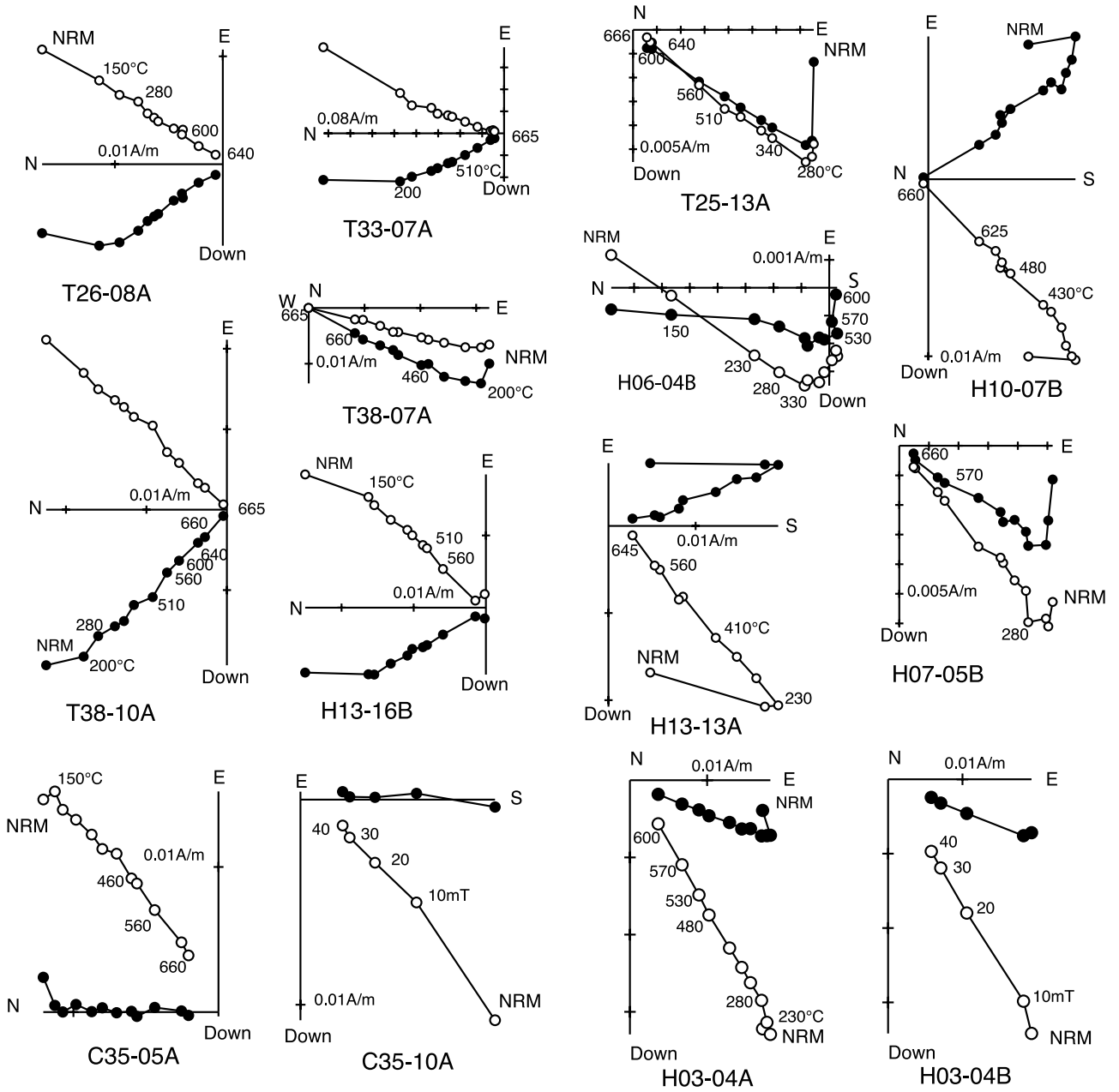

Figure 9. Orthogonal stepwise demagnetization diagrams for samples of fine-grained sediments from the Moquegua Group and Azapa Formation (Site C35). Thermal demagnetization usually removes a secondary overprint at 200–250°C. Thermal and AF demagnetizations of two specimens from the same core (H03-04 A and B) demonstrate that magnetite and hematite are the magnetic carriers of the ChRM. Same conventions as in Figure 5.

tization carried by the low magnetic coercivity phase has the same direction as the magnetization carried by hematite. This suggests that the magnetic carriers are mostly detrital magnetite and detrital hematite (Figure 9). The observation of normal and reverse polarities (Figures 9 and 10) also demonstrates that the ChRMs are acquired during deposition or very early diagenesis.

[70] Whereas most samples from sites in the MoqA and MoqB units are from red mudstones, the MoqC unit mostly consists of sandstones and conglomerates. Even though the sampling of the MoqC unit was restricted to the finest siltstones, the natural magnetization is overprinted by the recent field (sample H06-04B, Figure 9) and it was not possible to determine accurately primary characteristic magnetizations at sites H06 and H09.

5.2.1.1. Caravelí and Corral de Peña Localities

[71] Well-defined ChRMs of reverse polarity were determined at sites H3, H4 and H7 (Figure 10a). The site-mean

direction at site H5 was determined by combining line vectors and planes. Taking into account that sites H3, H4 and H5 are close to each other, these three sites were combined to provide a locality mean. Even though bedding attitude is almost horizontal, there is a slight decrease in dispersion upon tilt correction. The direction determined at site H7 (124.1, 44.7) located about 25 km southwest of Caravelí is similar to the Caravelí locality-mean direction (121.4, 28.3).

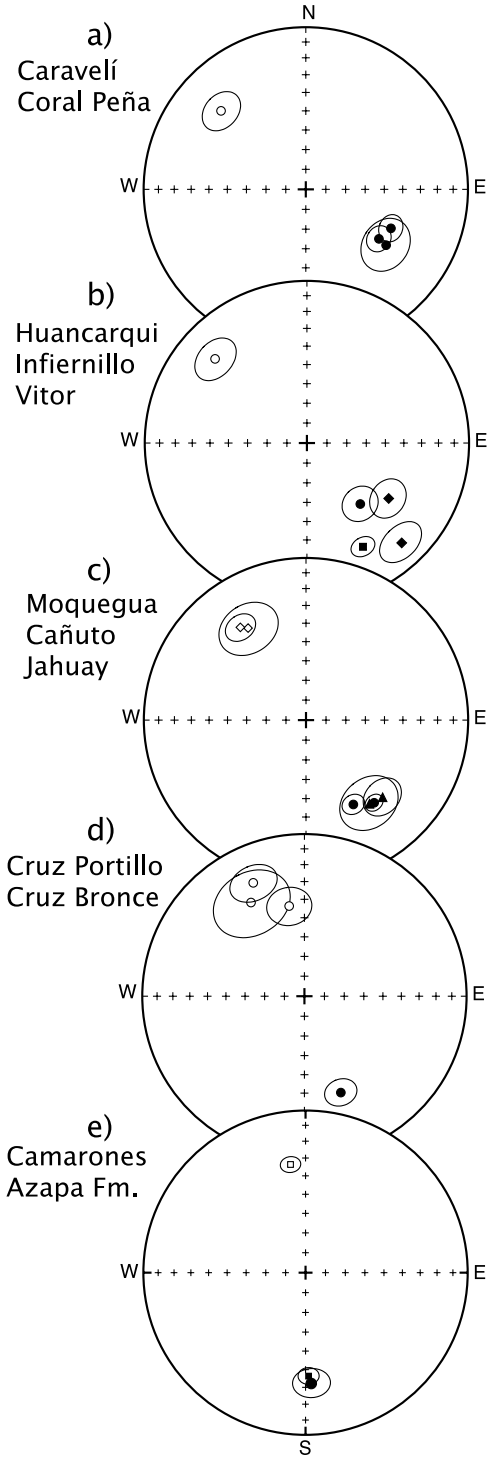

5.2.1.2. Aplao Valley

[72] Sites T24 and T25 (MoqA unit) are respectively of normal and reverse polarities (Figure 10b). All samples were combined to provide a locality mean (Huancarqui: 131.3, 35.5). At site T26 (Infiernillo), a reverse-normal-reverse polarity sequence is observed in a 20-m-thick sequence. There is a 21.3° difference in paleomagnetic declination between the Huancarqui (MoqA unit) and Infiernillo localities (151.6, 28.1; MoqC unit).

5.2.1.3. Vítor

[73] Paleomagnetic results from the two sites (H10 and T38) drilled at the Vítor locality were combined in a single locality mean. While only reverse polarity is observed at site H10, normal and reverse polarities are found at site T38.

5.2.1.4. Moquegua Region

[74] Reverse polarity is observed at sites T11 and T12 (Figure 10c). Because both sites are located in thick red mudstones of the upper MoqB unit, a locality mean was calculated combining all the characteristic directions. Normal polarity is observed at both sites T31 and T33 drilled in the small Jahuay basin (Figure 10c). At Cruz del Portillo (Figure 10d), the ChRM directions calculated from samples taken at 3 nearby sites (F29, T35 and T36) were combined to provide a locality mean. Dispersion is slightly higher than the one observed at Cruz del Bronce in the southern part of the wide Moquegua valley. At Cruz del Portillo, several samples were drilled in reworked tuffs, a few centimeters thick, and the highest dispersion may be due in part to geomagnetic secular variation.

5.2.1.5. Sama Valley

[75] The characteristic directions are of reverse polarity (Figure 10c) with a slightly lower dispersion than those observed at other localities.

5.2.1.6. Northernmost Chile

[76] Normal and reverse magnetizations were observed respectively at the top and base of the short section in the Azapa Formation at site 35 (Figure 10e). The magnetization is thus likely to be a detrital magnetization. *von Rotz et al.* [2005] published a magnetostratigraphic section from the same succession. Assuming that the coastal ignimbrite is the Oxaya main unit, *von Rotz et al.* [2005] indicate that the Azapa section was deposited in the time interval 20–23 Ma. However, this early Miocene age is likely to be a minimum age because evidence for erosion of the Azapa surface is found at site C93 and C94 below the coastal ignimbrite,

Figure 10. Equal-area stereonets of site-mean characteristic tilt-corrected directions in Paleogene sediments (results listed in Table 3). (a) Sites located near Caravelí and Corral de Peña. (b) Sites from Huancarqui, Infiernillo, and Vítor (circles). The square corresponds to site T26 from the Infiernillo locality. (c) Sites from the Jahuay locality (diamonds), Moquegua (circles), and Canuto (squares) localities. (d) Sites from the MoqC unit west (Cruz del Portillo locality) and south (Cruz del Bronce) of the Moquegua valley. (e) Results from the Azapa section, with squares corresponding to results obtained by *von Rotz et al.* [2005]. Same conventions as in Figure 7.

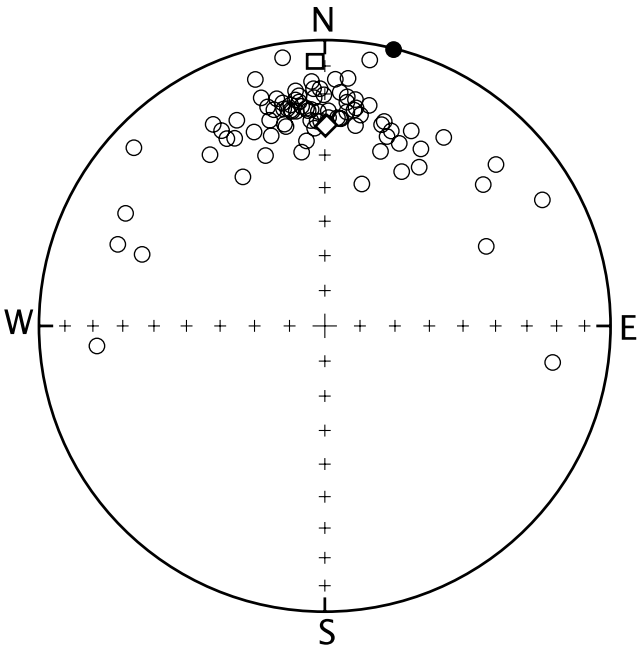

Figure 11. Equal-area projection of NRM directions showing a strong overprint in a normal field intermediate between the present-day field (square) and the average Brunhes field (diamond).

suggesting a hiatus exists between the ignimbrite and the Azapa sedimentary succession. We estimate that magnetization was acquired during the late Oligocene–early Miocene interval.

5.2.2. Coastal Southern Peru: The Camaná Group

[77] The magnetic susceptibility and intensity of remanent magnetization are an order of magnitude lower than values in the Moquegua Group (Figure 6). During thermal demagnetization, more than half of natural magnetization is demagnetized at very low temperature (MDT < 150°C). The normal polarity of NRMs suggests that this magnetization was acquired during the Brunhes period (Figure 11). Progressive thermal demagnetization did not identify a primary component. Recent coastal exposure may have favored oxidation of marine sediments and transformation of magnetic iron sulfides to magnetic iron oxide. Most sites from facially similar, northern time equivalents of the Camaná Group (Chilcatay (~ Camaná A) and Pisco (~ Camaná B) formations; ~14–15°S, ~75–78°W) also display mainly normal polarity [*Rousse et al.*, 2003]. However, *Rousse et al.* [2003] were able to extract a prefolding magnetization from samples of the Chilcatay formation.

5.3. Mesozoic and Paleocene Arc Rocks

5.3.1. Late Cretaceous–Paleocene Arc Rocks in Southern Peru

[78] *Roperch and Carlier* [1992] published preliminary results from the Late Cretaceous–Paleocene La Caldera batholith that crops out southwest of Arequipa. Here we combine these results with unpublished data from *Macedo-Sánchez* [1993] (Figure 12a and Table 4). The observed dispersion possibly results from internal deformation within this composite batholith. It is however important to observe that the mean direction for the batholith indicates a counterclockwise rotation of the same magnitude as that recorded by the subhorizontal MoqA or MoqB red beds at the nearby Vítor locality.

[79] Near the town of Moquegua, normal and reverse polarity magnetizations are observed in the Paleocene Toquepala volcanic rocks [*Macedo-Sánchez*, 1993] (Figure 12b and Table 4).

5.3.2. Jurassic to Paleocene Arc Rocks in Northernmost Chile

[80] Of the two sites drilled in Jurassic volcanics, only one (C21, Table 4) shows a well-defined ChRM. A secondary magnetization with unblocking temperatures in the range 200–500°C is identified at the other site C22 (Figure 13). This magnetization of normal polarity is different from the present-day field and has an inclination slightly higher than what would be expected in a Brunhes field overprint. Thermal demagnetization was not systematically used in the first studies on these Jurassic volcanics [*Palmer et al.*, 1980], and it may therefore be possible that secondary and primary magnetizations were not always well separated.

[81] In contrast with the complex behavior observed in Jurassic rocks, univectorial magnetizations were observed in Cretaceous rocks (Figure 13). Red sandstones (C23, Figure 13) sampled in the Lower Cretaceous Atajaña Formation have a normal polarity magnetization with maximum unblocking temperatures above 660°C, indicating that hematite is a significant magnetic carrier in these rocks. The six sites drilled in the volcanic Suca Formation at Quebrada Camarones have univectorial magnetizations of normal polarity in agreement with the mid-Cretaceous age of the unit (Figure 13). Moreover these volcanic rocks do not show evidence of petrologic alteration; we thus interpret this magnetization as a primary magnetization. Combining the six Suca sites and the two Atajaña sites provides a well-grouped mean direction with a positive fold test at 95% unfolding (Figures 12c and 12d). Near Esquiña (site C08), a normal polarity magnetization was observed in a Paleocene magmatic dike (Figure 13).

[82] Sites C62 and C63 were sampled in unnamed volcanodetritic sediments of Late Cretaceous or Paleocene age [*García*, 2002] in the Camiña area. At site C62, a single well-defined component of magnetization of reverse polarity is identified, whereas a more complex magnetization is observed at site C63 (Figure 13). The reverse polarity magnetization observed in the 210–460°C temperature range corresponds to the same direction as observed at site C63 in in situ coordinates. The high value of the Fisher parameter k at site C62 suggests that the magnetization is not a detrital magnetization. Taking into account that the overlying early Miocene ignimbrite (site C64) displays a normal polarity and no sign of remagnetization in a reverse field, it is likely that the reverse magnetization was acquired prior to the Neogene. We tentatively interpret the reverse polarity magnetization at sites C62 and C63 as a Paleocene-

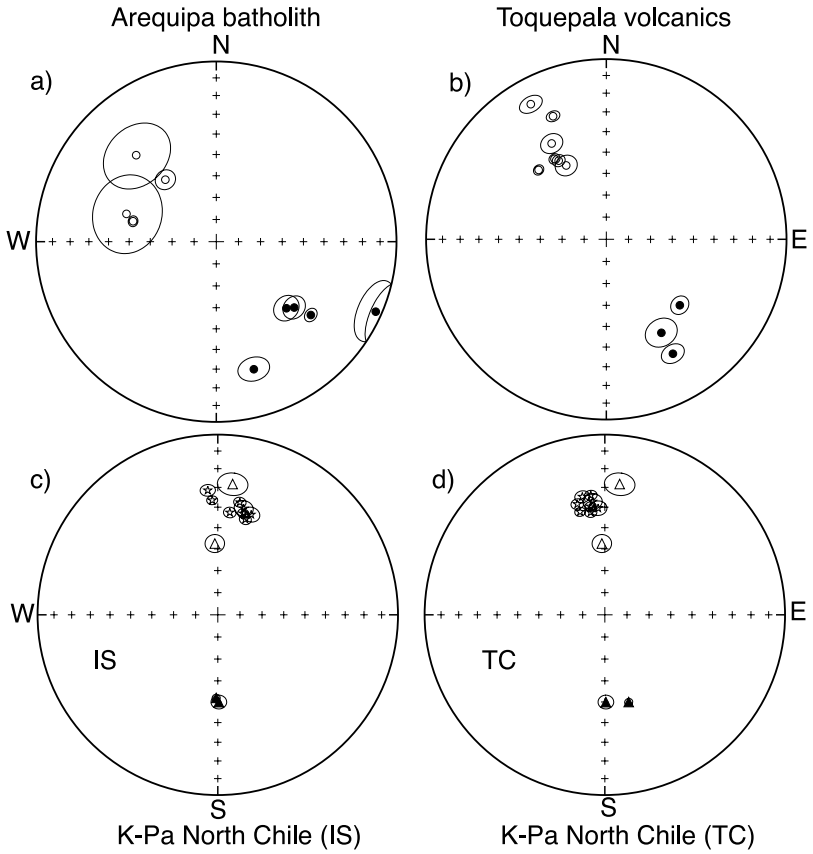

Figure 12. Equal-area plot of the characteristic directions in the Late Cretaceous Coastal Batholith near (a) Arequipa and (b) the Paleocene Toquepala volcanics. (bottom) Equal-area plots of the characteristic directions of sites in northern Chile. (c) In situ; (d) tilt-corrected. Stars correspond to Mesozoic sites and triangles to Paleogene sites. Open (solid) circles are projections onto the upper (lower) hemisphere.

Eocene secondary magnetization. Assuming that the remagnetization observed near Camiña is of early Paleogene age, we combine the paleomagnetic data from Camiña with the single result from Esquiña (Table 4).

6. Tectonic Rotations in the Central Andes: A Discussion

6.1. Southern Peruvian Fore Arc

[83] Our results evidence an overall SE-to-NW rotation gradient along the southern Peruvian fore arc, with amounts of counterclockwise rotation increasing from the Arica domain ($\sim 0^\circ$) to the Caravelí domain ($\sim -50^\circ$) (Table 5 and Figures 14 and 15). Rotations appear to be relatively homogeneous within each domain and to vary across domain boundaries (Figure 15), suggesting that this gradient reflects differential rotation between tectonic blocks.

[84] In northernmost Chile, the Mesozoic volcanics record a counterclockwise rotation ($-11.1 \pm 10.2^\circ$) that is not detected at the Paleogene locality of Camiña or in the late Oligocene sediments of the Azapa Formation. Lower Miocene ignimbrites do not appear to record any rotations ($R = 1.6 \pm 10.7^\circ$).

[85] In southern Peru, the large rotations reported by *Roperch and Carlier* [1992] in Mesozoic rocks of the southern Peruvian fore arc have rarely been taken into account in the interpretation of the formation of the Bolivian Orocline. Large counterclockwise rotations are now also observed in samples from the Moquegua Group (Table 5), with the largest occurring in the oldest units whereas their magnitude increases from southeast to northwest, reaching rotations $>50^\circ$ in the Caravelí domain. Such large rotations were first observed in primary magnetizations from Jurassic volcanics near Chala, in the western Caravelí domain (Figure 1b) [*Roperch and Carlier*, 1992]. The differences between the primary ($-70.5 \pm 16.1^\circ$) and secondary ($-37.3 \pm 10.4^\circ$) magnetizations in Jurassic volcanics at Chala could be due to an early Mesozoic component of rotation. However, the rotations recorded at Corral de Peña ($-52.9 \pm 8.5^\circ$) and Caravelí ($-55.6 \pm 7.0^\circ$) are not statistically different from the primary magnetization in the Jurassic taking into account the large uncertainty (16.1°). After tilt correction, the rotation determined from the secondary magnetizations ($-52.5 \pm 12.1^\circ$) is in better agreement with those recorded by the Moquegua Group near Caravelí. Further work is needed to test the hypothesis that part of the monoclinal tilt to the north of the Jurassic strata

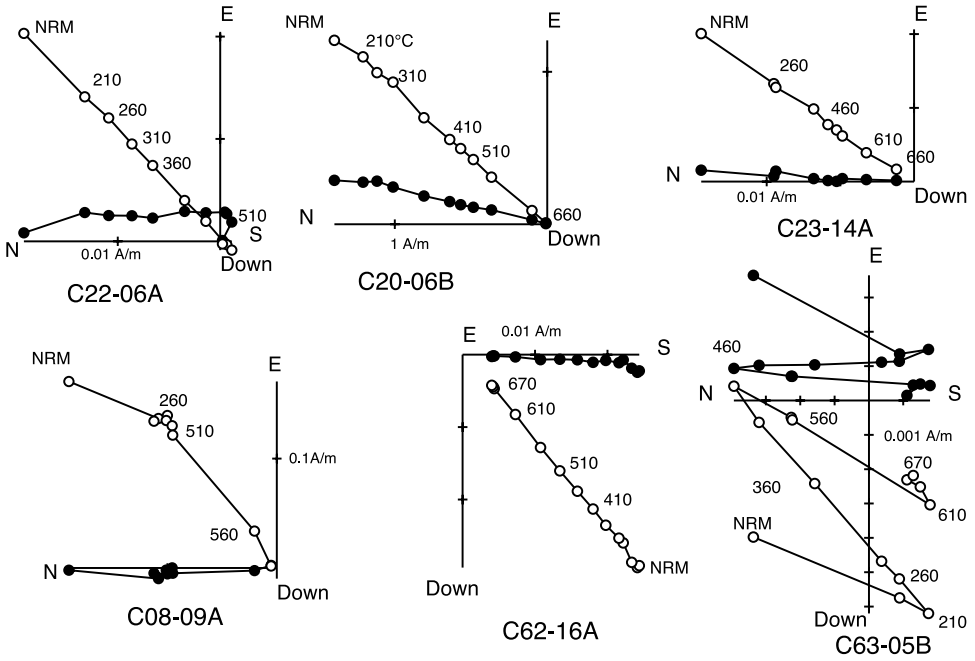

Figure 13. Orthogonal plots. Thermal demagnetization of samples from Mesozoic volcanics (samples C22-06A; C20-06B) and sandstones (C23-14A); sample C20-06B shows characteristic magnetizations with high unblocking temperatures, while sample C22-06A has a secondary component of magnetization in the temperature range 210–510°C, the age of which is uncertain and not considered in the present study; Eocene dike (sample C08-09A); Paleocene-Eocene red sandstones from the Camiña area (C62-16A and C63-05B). At site C63, a well-defined component of reverse polarity is identified in the temperature range 210–460°C. Same conventions as in Figure 5.

near Chala is of Tertiary age and postdates the acquisition of the secondary magnetization of Cretaceous age. In the Arequipa domain, the rotation recorded in the CB ($-43.9 \pm 14.7^\circ$) is similar to the rotation recorded by the subhorizontal MoqA or MoqB sediments at Vítor ($-46.9 \pm 8.7^\circ$). In the Moquegua domain, the rotations reported from in situ remagnetizations at Ilo (-31.4 ± 13.1) and La Yarada (-31.7 ± 11.5) [*Roperch and Carlier*, 1992] are in good agreement with the results in Paleocene volcanics and Eocene red bed deposits (Table 5). These observations imply that the fore arc of southern Peru underwent counterclockwise rotations after the middle to late Eocene, and do not support an earlier component of rotation. At this stage we cannot reject the hypothesis that rotations may have started slightly earlier in the Caravelí and Arequipa domains than in the Moquegua domain (Figure 15).

[86] Sites collected in the uppermost levels of the MoqB (Cruz del Bronce) and lowermost levels of the MoqC sediments, of early Oligocene age, record about half of the rotations recorded by the MoqA and MoqB units (Tables 3 and 5). Again, the largest rotations are observed in the northwestern region. South of Aplao (Arequipa domain), a counterclockwise rotation of $26.5 \pm 6.7^\circ$ is observed at site T26, which was sampled in fine-grained sediments intercalated in reworked tuffs and volcanoclastic sediments of the lower part of the MoqC unit, of late Oligocene age. The ignimbrite intercalated in the upper part of the MoqC unit ~200 m above site T26 is dated at 16.1 Ma. At Cruz del Portillo (Moquegua domain), the mean of 3 sites sampled in the MoqC unit below and above the ignimbrite dated at 25.5 ± 0.1 Ma, only indicates $13.9 \pm 10.7^\circ$ of counterclockwise rotation.

[87] The end of the rotation episode is difficult to constrain precisely (Figure 15). Although ignimbritic explosions were relatively common in the Miocene, the relatively low number of ignimbrite units does not allow a detailed sampling of secular variation. For this reason, paleomagnetic results in Miocene ignimbrites covering the fore arc from 15°S to 18°S were averaged for two time windows (25–16 Ma and 14–9 Ma), resulting in no evidence for counterclockwise rotations of the southern Peruvian fore arc during the Neogene from the 25–9 Ma ignimbrite record.

[88] The counterclockwise rotations recorded by Eocene-Oligocene red beds of the Moquegua Group confirm the major contribution of late Paleogene rotations in the central Andes. *Roperch et al.* [2000] suggested that rotations within the fore arc occurred during the Eocene, prior to the deformation in the back arc of the Andes. In central and northern Chile, obliquity of convergence could have resulted in dextral sinistral shear within the fore arc. In southern Peru, during the Eocene and Oligocene, it is unlikely that the obliquity had induced sinistral shear and counterclockwise related rotations along the fore arc, especially if the Arica bend was less pronounced before Andean

Table 5. Calculation of Rotation and Flattening[a]

Locality	Age, Ma	Latitude	Longitude	D, deg	I, deg	α_{95}	R, deg	∂R, deg	F, deg	∂F, deg
Caravelí	45	−15.816	−73.398	−58.6	−38.3	5.2	−55.6	7.0	−2.5	7.1
Corral de Peña	45	−15.892	−73.529	−55.9	−44.7	6.3	−52.9	8.5	3.8	7.6
Huancarqui	50	−16.116	−72.468	−48.7	−35.5	7.2	−45.8	8.0	−5.4	7.3
Infiernillo	25	−16.305	−72.430	−28.4	−28.1	5.4	−26.5	6.7	−10.3	7.4
Vitor	45	−16.474	−71.949	−49.7	−28.5	8.1	−46.9	8.7	−13.2	8.6
Arequipa	60	−16.500	−71.706	−50.9	−39.2	13.7	−43.9	14.7	2.9	12.1
Jahuay	40	−16.881	−70.917	−34.4	−31.5	5.7	−28.8	8.4	−12.0	8.8
Toquepala	60	−17.190	−70.920	−32.4	−38.5	7.8	−25.4	8.8	1.1	8.0
Moquegua	35	−17.212	−70.955	−42.4	−34.1	7.3	−37.2	8.1	−5.3	7.8
Canuto	40	−17.690	−70.482	−35.7	−36.8	3.8	−30.1	7.5	−7.8	8.0
Cruz del Bronce	30	−17.397	−71.021	−21.9	−32.9	6.2	−16.2	7.5	−4.7	7.9
Cruz del Portillo	25	−17.264	−71.163	−15.7	−40.8	9.1	−13.9	10.7	1.0	9.4
Ignimbrites 15–25 Ma	20	−17.100	−71.800	−1.9	−49.5	8.0	1.6	10.7	7.4	8.0
Ignimbrites 5–15 Ma	10	−17.000	−72.000	2.7	−37.8	10.8	5.2	11.3	0.6	9.4
Suca	100	−18.900	−70.000	351.2	−38.0	3.0	−11.1	10.2	3.1	14.1
Ignimbrites northern Chile	20	−18.700	−70.000	1.4	−36.9	6.5	4.7	8.2	−7.4	7.3
Camiña	50	−19.000	−69.45	1.7	−47.0	15.2	4.3	18.5	2.2	12.9
Azapa[b]	25	−19.084	−70.101	−4.3	−33.9	5.3	−1.4	9.1	−10.1	8.7

[a]Latitude and longitude are mean latitude and longitude of the locality; D, I, and α_{95} are observed paleomagnetic directions and confidence angle at 95%; R ± ∂R and F ± ∂F are rotation and flattening with respect to the reference South American apparent polar wander path of *Besse and Courtillot* [2002].
[b]The mean direction given in Table 3 is combined with the normal and reverse mean direction from *von Rotz et al.* [2005].

deformation. It is thus difficult to explain the rotations within the fore arc of southern Peru by in situ rotations of blocks within a sinistrally sheared domain. At several localities like Quebrada Corral de Peña (H7) or Vítor (H10, T38), sediments of the Moquegua Group are subhorizontal and overlie the basement. This indicates that rotations affect large mostly undeformed crustal blocks of the fore arc. These counterclockwise block rotations in the fore arc could not be accommodated in the neighboring WC and Altiplano because shortening in these areas has been apparently very low. The relative ages of the rotated sampled strata constrain the period of rotation to the latest Eocene–latest Oligocene interval (~35–25 Ma) (Figure 15), a time interval in better agreement with the onset of deformation in the Eastern Cordillera. *Lamb* [2001a] also indicated that the amounts of shortening needed to accommodate Paleogene rotations are difficult to account for by the shortening observed in the fore arc and volcanic arc alone, but could easily be accommodated by Eocene-Oligocene deformation in the Altiplano and the Eastern Cordillera. The Bolivian segment of the EC was indeed strongly shortened [*Sheffels*, 1990; *Baby et al.*, 1997; *Kley and Monaldi*, 1998; *McQuarrie*, 2002; *Müller et al.*, 2002] (Figures 14 and 16) at least from the late Oligocene to early middle Miocene [*Sempere et al.*, 1990] and possibly started in the late Eocene [*Horton*, 2005; *Elger et al.*, 2005]. Eocene/Oligocene shortening is also documented in central Peru [*Mégard*, 1978].

6.2. Northern Chilean Fore Arc

[89] In northern Chile between 22° and 28°S, clockwise tectonic rotations are widespread along the fore arc [*Randall et al.*, 1996, 2001; *Arriagada et al.*, 2000, 2003, 2006], whereas the few paleomagnetic data from Neogene rocks [*Somoza et al.*, 1999; *Somoza and Tomlinson*, 2002] do not show rotations. *Taylor et al.* [2005] suggested that rotations in Chile were related to late Paleocene–early Eocene highly oblique convergence. However, *Arriagada et al.* [2006] reported rotations also in Eocene rocks and argued that rotations in Chile cannot be explained by local deformation only, but that significant shortening in the back arc is needed to enable the rotations of large fore-arc blocks. Dextral displacements and clockwise rotations along the Chilean fore arc need to be accommodated by some northeastward displacement of the fore arc of northernmost Chile and southern Peru. A counterclockwise rotation of the Peruvian fore arc accompanying a major bending of the orocline could provide the space needed to accommodate the rotations along the Chilean fore arc (Figure 16). Although little documented, the amount of Paleogene shortening across the Puna plateau is estimated to be less than in the Bolivian Andes. The resulting along-strike gradient in horizontal shortening associated with contemporaneous deformation in the Precordillera of northern Chile could also explain the clockwise rotations in the neighboring fore arc [*Arriagada et al.*, 2003, 2006]. This late Eocene–early Miocene, early period of Andean building thus appears to coincide with the principal period of oroclinal bending in the fore arc. Although most previous interpretations of the Bolivian Orocline have focused on the "Arica bend" [e.g., *Beck*, 1998], the largest rotations appear to be recorded northwest of Arequipa (counterclockwise) and south of 22°S (clockwise), indicating that the apparent bend marked by the coastline near Arica is not the hinge of the Bolivian Orocline, and tending to confirm *Gephart*'s [1994] analysis.

6.3. Other Regions of the Bolivian Orocline

[90] Large counterclockwise rotations are documented in pre-Oligocene rocks of the northern Altiplano in Peru and Bolivia [*Gilder et al.*, 2003; *Butler et al.*, 1995; *Richards et*

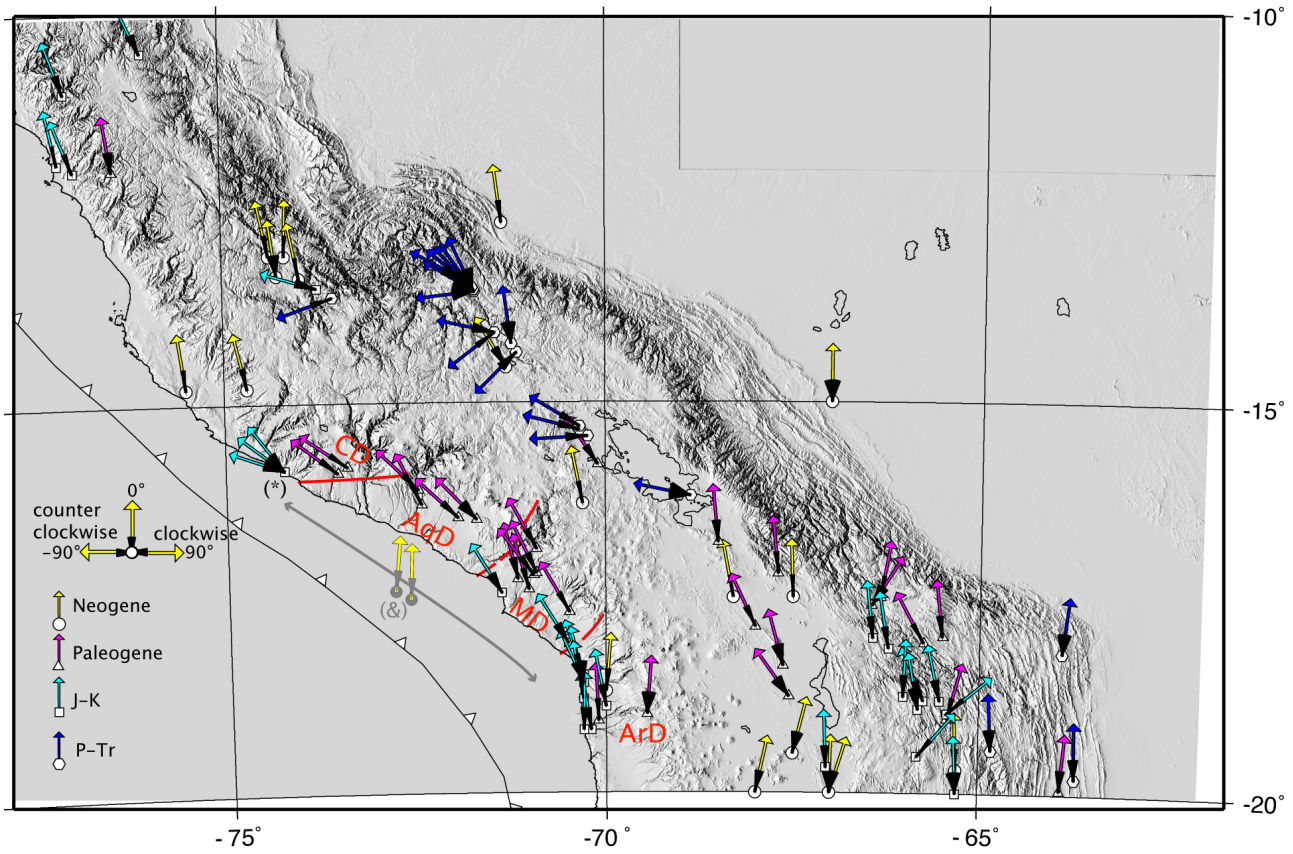

Figure 14. Compilation of tectonic rotations within the central Andes. J-K, Jurassic-Cretaceous. P-Tr, Permian-Trias. Black dots correspond to results from the present study. Asterisk is to rotations near the Chala locality that were calculated on the basis of primary magnetizations in Jurassic volcanics and remagnetization data [*Roperch and Carlier*, 1992] (the lesser rotations are in situ and the larger are tilt-corrected). Ampersand is to Neogene rotations that correspond to paleomagnetic results from spatially distributed sites in 25–9 Ma ignimbrites; the location of these two localities is thus arbitrary in this fore-arc segment. CD, Caravelí domain; AqD, Arequipa Domain; MD, Moquegua domain; ArD, Arica domain. Rotations are listed in the auxiliary material.

al., 2004]. *Gilder et al.* [2003] reported large rotations in Late Paleozoic–Early Mesozoic rocks of the EC of southern Peru (Figure 14) and proposed a post-middle Oligocene origin of the paleomagnetic rotations. Data from Paleocene sediments [*Butler et al.*, 1995; *Lamb*, 2001a; *Richards et al.*, 2004]) confirm that a significant fraction of the counterclockwise rotations recorded by Paleozoic rocks, if not all, is post-Paleocene. Whereas Paleogene rocks record counterclockwise rotations up to 50°, except at a few places [*Rousse et al.*, 2005], only ~10° of rotation is documented in late Miocene rocks from the northern Altiplano. This is in agreement with our hypothesis that rotations along the fore arc are also contemporaneous with deformation and rotations in the back arc.

[91] In the central Andes, there is however generally a link between paleomagnetic rotations and structural trends [e.g., *Coutand et al.*, 1999; *Lamb*, 2001a], and large rotations are generally associated with wrench zones. However, unless paleomagnetic results concern a large and simple structure, as the Corque syncline in the northern Altiplano, it can be complicated to use apparent paleomagnetic rotations to constrain along-strike gradients in shortening. The complex and often low-wavelength upper crustal deformation in the Altiplano-Puna and EC makes it more difficult than usually thought to properly understand the meaning of the paleomagnetic results.

[92] Several authors have reported middle to late Miocene rotations in the back arc of the central Andes [*Heki et al.*, 1985b; *Roperch et al.*, 1999; *Rousse et al.*, 2002; *Barke et al.*, 2004; *MacFadden et al.*, 1995], but in most cases the magnitude of these rotations does not exceed 10°.

[93] The late Neogene ~10° counterclockwise rotation near Ayacucho (south central Peru), first observed in the Miocene Ocros dike swarm [*Heki et al.*, 1985b] was confirmed in middle Miocene sediments of the Ayacucho basin, whereas data from overlying upper Miocene sediments suggested that the rotation was achieved prior to 7 Ma [*Rousse et al.*, 2002]. Farther south, in the northern

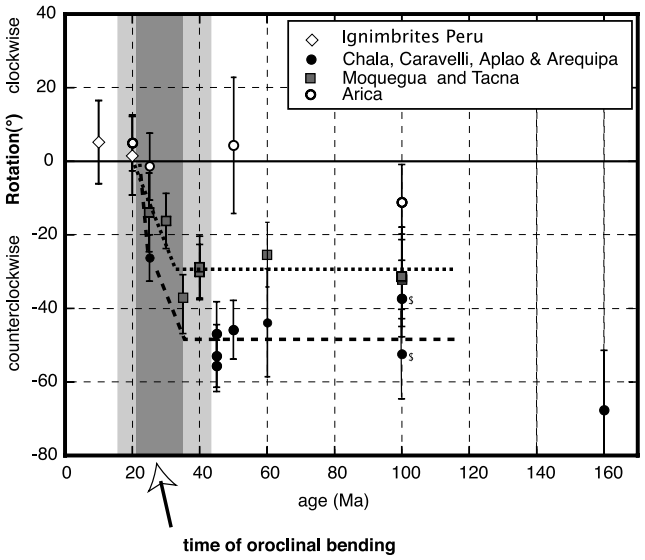

Figure 15. Plot of the magnitude of tectonic rotations versus the age of magnetization. Because of the apparent northwestward gradient in counterclockwise rotation, three areas are highlighted. South of Arica, there is no significant rotation. Rotations from Arequipa to Caravelí and Chala are larger than those between Tacna and Moquegua. Results from southern Peru indicate that most of the rotations within the fore arc occurred between 40–35 Ma and 20–15 Ma. Since 15 Ma, the curvature of the Arica bend has not been enhanced. Dollar sign indicates rotation deduced from the Chala remagnetizations is shown as in situ and after tilt correction. The dark grey box highlights the proposed time interval for oroclinal bending, starting in the latest Eocene–earliest Oligocene and finishing in the latest Oligocene. The light grey boxes illustrate the uncertainties. Oroclinal bending could have started earlier in the Arequipa and Caravelí domains and possibly ended in the early Miocene.

Bolivian Altiplano, the Corque syncline is a large and wide structure rotated counterclockwise by ~10° [*Roperch et al.*, 1999]. Geochronologic and magnetostratigraphic data indicate that the rotation of the Corque syncline is younger than 9 Ma. *Roperch et al.* [2000] reinterpreted paleomagnetic directions from Devonian through Late Permian strata of the EC and sub-Andes of Bolivia [*Libarkin et al.*, 1998] as acquired during the Permo-Carboniferous reversed-polarity superchron. Following exclusion of results from one locality of *Libarkin et al.* [1998], *Roperch et al.* [2000] and *Gilder et al.* [2003] observed that maximum clustering of paleomagnetic directions from Paleozoic rocks in the southern sub-Andes of Bolivia clearly occurs at 100% unfolding, indicating that Paleozoic strata acquired their characteristic magnetization prior to folding. *Roperch et al.* [2000] then used these directions to determine Tertiary vertical axis rotations for the sub-Andes. Because of uncertainties in the age of the magnetizations and thus in the pole of reference, *Richards et al.* [2004] argued that determining Neogene vertical axis rotations in the sub-Andes using the data reported by *Libarkin et al.* [1998] was unjustified. However, results obtained in Oligo-Miocene sedimentary strata of the sub-Andes by *Lamb* [2001a] are in good agreement with the rotations calculated by *Roperch et al.* [2000], and we believe that these rotations do indeed represent late Neogene clockwise rotations acquired while shortening was propagating eastward in the southern sub-Andes.

[94] Paleomagnetic data from the eastern Bolivian Andes have been interpreted as evidence for the progressive enhancement of the curvature during Cenozoic fold-thrust belt deformation [*Richards et al.*, 2004]. However, late Neogene oroclinal deformation of the eastern Bolivian Andes does not necessarily imply rotations within the fore arc. From the middle Miocene to present, propagation of deformation in the inter-Andean zone and sub-Andes is likely to have involved large rotations on thrust faults. *Coutand et al.* [1999] showed that a close relationship exists between the paleomagnetic rotations and the orientations of major fold axes and thrust faults. As already pointed out by *Lamb* [2001a], NW striking major fault zones in the northern limb of the orocline and conjugate dextral NE striking faults in the southern central Andes induce rotations in the sheared area [*Rousse et al.*, 2005]. Apparent oroclinal curvature of the eastern Andean front can thus occur during the late Neogene while the fore arc is moving eastward without significant enhancement of the Arica bend.

6.4. Central Peru and Northern Peru

[95] Did counterclockwise rotations along the Peruvian Andes develop during different time intervals, and, most important, following distinct mechanisms? *Rousse et al.* [2003] found counterclockwise rotations in the Cajabamba basin and in the Callejón de Huaylas basin, which lies west of the Cordillera Blanca batholith. *Rousse et al.* [2003] argued that the counterclockwise rotations previously reported in northern and central Peru [*Mitouard et al.*, 1992; *Macedo-Sánchez et al.*, 1992a, 1992b] have been a consequence of the north-to-south sweeping of the margin by the Nazca ridge since 11–10 Ma. The large counterclockwise rotations reported here in southern Peru cannot however be explained by the displacement and collision of the Nazca ridge because this oceanic feature has not reached the southern Peruvian fore arc yet. Furthermore, our data indicate that rotations in southern Peru occurred between the latest Eocene and latest Oligocene.

[96] *Rousse et al.* [2003] reported paleomagnetic results from two small Neogene basins east of Cajamarca, northern Peru. The Cajabamba basin records a counterclockwise rotation that does support the hypothesis of late Neogene rotation [*Rousse et al.*, 2003]. However, the nonrotated San Marcos basin extends across anomalous, WNW trending structures where an angular unconformity is bracketed between ~44 and ~39 Ma [*Noble et al.*, 1990], and where >20° counterclockwise rotations are recorded in Cretaceous limestones [*Mitouard et al.*, 1992] and Paleogene volcanics [*Mitouard et al.*, 1990]. The nonrotated San Marcos basin may indeed indicate that Paleogene volcanics were rotated prior to the Miocene. In a large part of northern Peru,

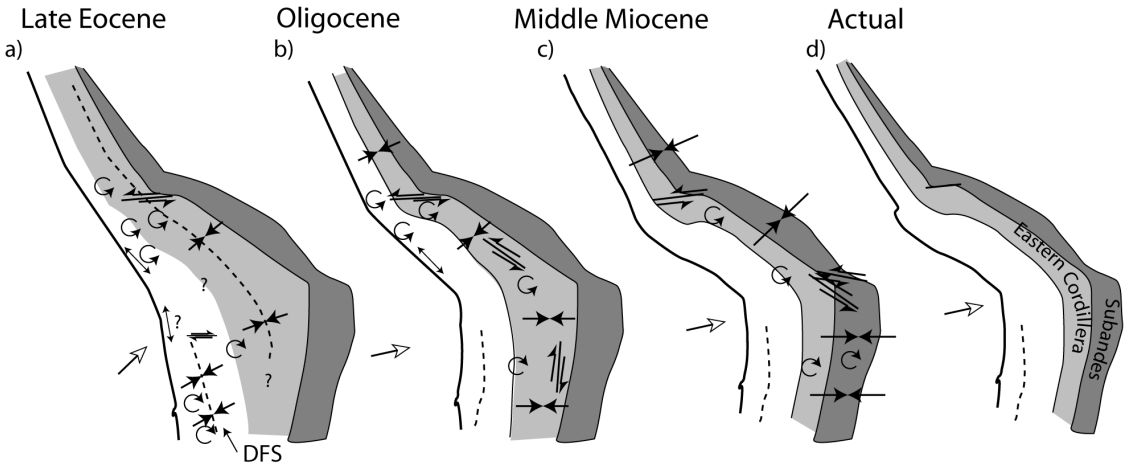

Figure 16. Schematic geodynamic evolution of the Bolivian Orocline. From the late Eocene to Oligocene, deformation developed in the EC and in the Domeyko Fault System (DFS) of northernmost Chile. Deformation in the Abancay region produced large counterclockwise rotations within the fore arc of southern Peru. From the middle Miocene to present, shortening was restricted to the inter-Andean and sub-Andean zones with no significant rotation along the fore arc.

significant shortening occurred from the Eocene to the early Miocene in the Marañon fold-and-thrust belt [*Mégard*, 1978; *Noble et al.*, 1990] and rotations may well have been produced during this shortening. Thus at least some rotations in northern Peru may in fact have been approximately contemporaneous of rotations in southern Peru, and acquired during major deformation of the WC and EC. Further work is needed to test the hypothesis that late Neogene rotations in northern Peru correspond to small block rotations, in contrast with the possibly >20° late Paleogene counterclockwise rotation of an important tract of the fore arc (6–8°S) suggested by the paleomagnetic data reported by *Mitouard et al.* [1990, 1992].

6.5. Abancay Deflection

[97] One of the most striking structural features in southern Peru is the Abancay deflection, which is clearly marked in the present-day topography (Figure 1a) and in the geology (Figure 1b), and has apparently been a major heterogeneity in the Peruvian Andes since the Paleozoic [*Sempere et al.*, 2002]. Toward the coastal area, the coastal batholith trend clearly bears an inflection point that defines the Caravelí deflection; less pronounced than the Abancay deflection, it is nevertheless somewhat parallel to it and can be considered as its southern ''sister'' deflection (Figure 1b). We propose that the Abancay and Caravelí deflections together mark the northwestern boundary of the Bolivian Orocline, and, because the oldest and largest forearc rotations are recorded from the Caravelí deflection, that the orocline started to develop when these sister deflections began to form.

[98] The subducted Nazca ridge, which currently marks the limit between normal to flat subduction, approximately underlies the Abancay deflection, but not the Caravelí deflection (Figure 1). The Nazca Ridge started at ~11.2–10 Ma to be subducted beneath South America at 11–10°S, and has swept the margin southward to achieve its current position [*Hampel*, 2002; *Rousse et al.*, 2003]. The Abancay deflection and associated rotations thus predate the subduction of the Nazca ridge at this latitude. The present-day deep slab (>500 km) presents a sharp ''sinistral'' deflection (= NE down) near 14°S, where the slab is striking WNW and dips ~60° to the NNE (Figure 1a). This very deep deflection occurs ~500 km east of the shallow, crustal Abancay deflection and the question arises whether the two are genetically related. *James and Sacks* [1999] proposed that a slab transition from normal to flat slab subduction in late Eocene/early Oligocene was coincident with extensive crustal deformation in the eastern Altiplano and EC. The formation of the Abancay deflection and the counterclockwise rotations fit well in this model.

6.6. Interpretations of GPS Data

[99] Preliminary GPS data [*Norabuena et al.*, 1998; *Bevis et al.*, 1999, 2001; *Bevis and Martel*, 2001] have been used to support the hypothesis that shortening increased with decreasing relative convergence between the Nazca and South American plates [*Lamb*, 2000, 2001a, 2001b; *Hindle et al.*, 2002]. One of the major difficulties in estimating the strain rate in the back arc from GPS data is the modeling of the seismic cycle. *Allmendinger et al.* [2005] argued that even though a significant part of the instantaneous deformation field is probably elastic and due to interseismic locking of the plate boundary, some of the interseismic deformation field must reflect permanent deformation, and/or some of the current elastic deformation will be converted to upper plate permanent deformation over time rather than be recovered by elastic rebound during interplate earthquakes. The largest rotation derived from the GPS data is found in the fore arc of southern Peru. When extrapolated to

geological time, a 16° counterclockwise rotation would be expected for the last 10 Myr. The apparent discrepancy between the lack of rotation recorded by the ignimbrites and the GPS-deduced rotations is probably due to the fact that only ~10% of the GPS velocity will be converted into permanent crustal deformation [*Allmendinger et al.*, 2005]. Therefore the rotation rates calculated from GPS stations located in the fore arc should be an order of magnitude smaller and thus in agreement with the paleomagnetic data.

[100] *Khazaradze and Klotz* [2003] reevaluated the whole data set for the central Andes and found shortening in the back arc to be less than 5 mm/yr, a value similar to the previous estimate by *Klotz et al.* [2001]. On the other hand, *Brooks et al.* [2003] found that the back arc creeps continuously at 4.5 mm/yr in the latitude range 26–36°S. We speculate that GPS data may indicate very little present-day along-strike shortening gradient in the Andes in contrast to the pre-Miocene shortening gradient needed to account for the large rotations recorded in the fore arc.

7. Conclusions

[101] Paleomagnetic results obtained in Eocene-Oligocene sediments of the Moquegua Group evidence a spatial gradient of rotations in southern Peru, between ~0° recorded in the southeast (Arica domain) and up to 50° counterclockwise rotations in the northwest (Caravelí domain). Ignimbrites younger than 25 Ma do not show evidence for rotations within the fore arc. Amounts of rotations are apparently homogeneously distributed within each of the four recognized tectonic domains, and vary across domain boundaries. The relative ages of the rotated sampled strata constrain the period of time during which rotations developed to the latest Eocene–latest Oligocene interval (~35–25 Ma).

[102] A major episode of oroclinal bending thus developed in the fore arc of southern Peru during approximately the Oligocene. Because of the lack of evidence for coeval significant shortening in the fore arc, arc (WC) or Altiplano, we propose that rotations within the fore arc were accommodated by significant shortening in the Eastern Cordillera. In southern Peru, wrenching within the EC along the Abancay deflection accommodated oroclinal bending of the fore arc in the Caravelí deflection.

[103] The paleomagnetic data indicate that, along its Pacific side, the Bolivian Orocline was formed during the latest Eocene – earliest Miocene interval, i.e., a rather long period of time. This finding suggests major pre-Neogene mountain building and apparently disagrees with claims [*Hindle et al.*, 2002] that shortening in the Bolivian Orocline increased with decreasing convergence during the Neogene.

[104] **Acknowledgments.** Financial support was principally provided by IRD. César Arriagada acknowledges funding from CONICYT (FONDECYT projects 1970002 and 3030050). Tony Monfret provided advice on interpretation of seismological data and a database of relocated earthquake hypocenters. Jorge Barriga (Universidad Jorge Basadre Grohmann, Tacna) participated in field works in the Tacna and Moquegua areas. P.R. and T.S. acknowledge fruitful discussions with Gabriel Carlier on the geology of southern Peru. During field sampling, we appreciated the help from Sergio Villagrán in Chile and from José Berrospi and Manuel Lara in Peru. Comments by Stuart Gilder and Graeme Taylor led to many improvements. Contribution UMR Geosciences Azur 801.

References

Allmendinger, R. W., R. Smalley Jr., M. Bevis, H. Caprio, and B. A. Brooks (2005), Bending the Bolivian orocline in real time, *Geology*, *33*, 905–908.

Arriagada, C., P. Roperch, and C. Mpodozis (2000), Clockwise block rotations along the eastern border of the Cordillera de Domeyko, northern Chile (22°45′–23°30′S), *Tectonophysics*, *326*, 153–171.

Arriagada, C., P. Roperch, C. Mpodozis, G. Dupont-Nivet, P. R. Cobbold, A. Chauvin, and J. Cortes (2003), Paleogene clockwise tectonic rotations in the forearc of central Andes, Antofagasta region, northern Chile, *J. Geophys. Res.*, *108*(B1), 2032, doi:10.1029/2001JB001598.

Arriagada, C., P. Roperch, C. Mpodozis, and R. Fernández (2006), Paleomagnetism and tectonics of the southern Atacama Desert, (25°–28°S) northern Chile, *Tectonics*, doi:10.1029/2005TC001923, in press.

Aubry, L., P. Roperch, M. Urreiztieta, E. Rossello, and A. Chauvin (1996), Paleomagnetic study along the southeastern edge of the Altiplano-Puna Plateau: Neogene tectonic rotations, *J. Geophys. Res.*, *101*, 17,883–17,899.

Baby, P., G. Herail, R. Salinas, and T. Sempere (1992), Geometry and kinematic evolution of passive roof duplexes deduced from cross section balancing: Example from the foreland thrust system of the southern Bolivian sub-Andean Zone, *Tectonics*, *11*, 523–536.

Baby, P., P. Rochat, G. Mascle, and G. Hérail (1997), Neogene shortening contribution to crustal thickening in the back arc of the central Andes, *Geology*, *25*, 883–886.

Barke, R., M. Niocaill, and S. H. Lamb (2004), Oroclinal bending in the Bolivian Andes: New evidence for post 10 Ma rotations linked to shortening gradients in the fold-and-thrust belt, *Eos Trans. AGU*, *85*(47), Fall Meet. Suppl., Abstract GP42A-06.

Beck, M. E. (1998), On the mechanism of crustal block rotations in the central Andes, *Tectonophysics*, *299*, 75–92.

Beck, S. L., and G. Zandt (2002), The nature of orogenic crust in the central Andes, *J. Geophys. Res.*, *107*(B10), 2230, doi:10.1029/2000JB000124.

Bellon, H., and C. Lefevre (1976), Données géochronologiques sur le volcanisme andin dans le sud Pérou. Implications volcanotectoniques, *C. R. Acad. Sci.*, *283*, 1–4.

Besse, J., and V. Courtillot (2002), Apparent and true polar wander and the geometry of the geomagnetic field over the last 200 Myr, *J. Geophys. Res.*, *107*(B11), 2300, doi:10.1029/2000JB000050.

Bevis, M., and S. J. Martel (2001), Oblique plate convergence and interseismic strain accumulation, *Geochem. Geophys. Geosyst.*, *2*(8), doi:10.1029/2000GC000125.

Bevis, M., E. C. Kendrick, R. Smalley Jr., T. Herring, J. Godoy, and F. Galban (1999), Crustal motion north and south of the Arica deflection: Comparing recent geodetic results from the central Andes, *Geochem. Geophys. Geosyst.*, *1*(1), doi:10.1029/1999GC000011.

Bevis, M., E. Kendrick, R. Smalley Jr., B. Brooks, R. Allmendinger, and B. Isacks (2001), On the strength of interplate coupling and the rate of back arc convergence in the central Andes: An analysis of the interseismic velocity field, *Geochem. Geophys. Geosyst.*, *2*(11), doi:10.1029/2001GC000198.

Brooks, B. A., M. Bevis, R. Smalley Jr., E. Kendrick, R. Manceda, E. Lauría, R. Maturana, and M. Araujo (2003), Crustal motion in the southern Andes (26°–36°S): Do the Andes behave like a microplate?, *Geochem. Geophys. Geosyst.*, *4*(10), 1085, doi:10.1029/2003GC000505.

Butler, R. F., D. R. Richards, T. Sempere, and L. G. Marshall (1995), Paleomagnetic determinations of vertical-axis tectonic rotations from Late Cretaceous and Paleocene strata of Bolivia, *Geology*, *23*, 799–802.

Cecioni, G. O., and A. Garcia (1960), Stratigraphy of coastal range in Tarapaca Province, Chile, *Am. Assoc. Pet. Geol. Bull.*, *44*, 1609–1620.

Clark, A. H., et al. (1990), Geologic and geochronologic constraints on the metallogenic evolution of the Andes of Southeastern Peru, 1990, *Econ. Geol.*, *85*, 1520–1583.

Coutand, I., P. Roperch, A. Chauvin, P. R. Cobbold, and P. Gautier (1999), Vertical axis rotations across the Puna plateau (northwestern Argentina) from paleomagnetic analysis of Cretaceous and Cenozoic rocks, *J. Geophys. Res.*, *104*, 22,965–22,984.

Elger, K., O. Oncken, and J. Glodny (2005), Plateau-style accumulation of deformation: Southern Altiplano, *Tectonics*, *24*, TC4020, doi:10.1029/2004TC001675.

Farías, M., R. Charrier, D. Comte, J. Martinod, and G. Herail (2005), Late Cenozoic deformation and uplift of the western flank of the Altiplano: Evidence from the depositional, tectonic, and geomorphologic evolution and shallow seismic

activity (northern Chile at 19°30′S), *Tectonics*, *24*, TC4001, doi:10.1029/2004TC001667.

Fisher, R. A. (1953), Dispersion on a sphere, *Proc. R. Soc. London, Ser. A*, *217*, 275–305.

García, M. (2002), Evolution Oligo-Néogène de l'Altiplano Occidental (arc et avant-arc des Andes d'Arica, 18°–19°S): Tectonique, volcanisme, sédimentation, géomorphologie et bilan érosion-sédimentation?, thèse d'université, 178 pp., Univ. Joseph Fourier, Grenoble, France.

García, M., and G. Hérail (2001), Comment on 'Geochronology (Ar-Ar, K-Ar and He-exposure ages) of Cenozoic magmatic rocks from northern Chile (18–22°S): Implications for magmatism and tectonic evolution of the central Andes' (2000), *Rev. Geol. Chile*, *28*, 127–130.

García, M., and G. Hérail (2005), Fault-related folding, drainage network evolution and valley incision during the Neogene in the Andean Precordillera of northern Chile, *Geomorphology*, *65*, 279–300.

Gephart, J. W. (1994), Topography and subduction geometry in the central Andes: Clues to the mechanics of a noncollisional orogen, *J. Geophys. Res.*, *99*, 12,279–12,288.

Gerbault, M., J. Martinod, and G. Herail (2005), Possible orogeny-parallel lower crustal flow and thickening in the central Andes, *Tectonophysics*, *399*, 59–72.

Gilder, S., S. Rousse, D. Farber, T. Sempere, V. Torres, and O. Palacios (2003), Post-Middle Oligocene origin of paleomagnetic rotations in Upper Permian to Lower Jurassic rocks from northern and southern Peru, *Earth Planet. Sci. Lett.*, *210*, 233–248.

Gregory-Wodzicki, K. M. (2000), Uplift history of the central and northern Andes: A review, *Geol. Soc. Am. Bull.*, *112*, 1091–1105.

Gutscher, M.-A., J.-L. Olivet, D. Aslanian, J.-P. Eissen, and R. Maury (1999), The "lost Inca Plateau": Cause of flat subduction beneath Peru?, *Earth Planet. Sci. Lett.*, *171*, 335–341.

Hampel, A. (2002), The migration history of the Nazca Ridge along the Peruvian active margin: a re-evaluation, *Earth Planet. Sci. Lett.*, *203*, 665–679.

Heki, K., Y. Hamano, and M. Kono (1983), Rotation of the Peruvian block from palaeomagnetic studies of the central Andes, *Nature*, *305*, 514–516.

Heki, K., Y. Hamano, and M. Kono (1985a), Paleomagnetic study of the Cretaceous Atajaña Formation and the Arica Dike swarm, northernmost Chile, *J. Geomagn. Geoelectr.*, *37*, 107–117.

Heki, K., Y. Hamano, M. Kono, and T. Ui (1985b), Palaeomagnetism of Neogene Ocros dyke swarm, The Peruvian Andes: Implication for the Bolivian orocline, *Geophys. J. R. Astron. Soc.*, *80*, 527–534.

Hindle, D., J. Kley, E. Klosko, S. Stein, T. Dixon, and E. Norabuena (2002), Consistency of geologic and geodetic displacements during Andean orogenesis, *Geophys. Res. Lett.*, *29*(8), 1188, doi:10.1029/2001GL013757.

Hindle, D., J. Kley, O. Oncken, and S. Sobolev (2005), Crustal balance and crustal flux from shortening estimates in the central Andes, *Earth Planet. Sci. Lett.*, *230*, 113–124.

Horton, B. K. (2005), Revised deformation history of the central Andes: Inferences from Cenozoic foredeep and intermontane basins of the Eastern Cordillera, Bolivia, *Tectonics*, *24*, TC3011, doi:10.1029/2003TC001619.

Huamán, D. (1985), Evolution tectonique cénozoique et néotectonique du piémont pacifique dans la région d'Aréquipa (Andes du Sud du Pérou), thèse 3ème cycle, 220 pp., Univ. Paris XI, Orsay, France.

Husson, L., and T. Sempere (2003), Thickening the Altiplano crust by gravity-driven crustal channel flow, *Geophys. Res. Lett.*, *30*(5), 1243, doi:10.1029/2002GL016877.

Isacks, B. (1988), Uplift of the central Andean plateau and bending of the Bolivian orocline, *J. Geophys. Res.*, *93*, 3211–3231.

James, D. E., and S. Sacks (1999), Cenozoic formation of the Central Andes: A geophysical perspective, in *Geology and Ore Deposits of Central Andes, Spec. Publ.*, vol. *7*, edited by B. J. Skinner, pp. 1–25, Soc. of Econ. Geol., Littleton, Colo.

Kennan, L. (2000), Large-scale geomorphology in the central Andes of Peru and Bolivia: To tectonic; magmatic and climatic processes, in *Geomorphology and Global Tectonics*, edited by M. A. Summerfield, pp. 167–199, John Wiley, Hoboken, N. J.

Khazaradze, G., and J. Klotz (2003), Short- and long-term effects of GPS measured crustal deformation rates along the south central Andes, *J. Geophys. Res.*, *108*(B6), 2289, doi:10.1029/2002JB001879.

Kirschvink, J. L. (1980), The least-squares line and plane and the analysis of paleomagnetic data, *Geophys. J. R. Astron. Soc.*, *62*, 699–718.

Kley, J., and C. R. Monaldi (1998), Tectonic shortening and crustal thickness in the Central Andes: How good is the correlation?, *Geology*, *26*, 723–726.

Klotz, J., G. Khazaradze, D. Angermann, C. Reigber, R. Perdomo, and O. Cifuentes (2001), Earthquake cycle dominates contemporary crustal deformation in central and southern Andes, *Earth Planet. Sci. Lett.*, *193*, 437–446.

Lamb, S. (2000), Active deformation in the Bolivian Andes, South America, *J. Geophys. Res.*, *105*, 25,627–25,653.

Lamb, S. (2001a), Vertical axis rotation in the Bolivian orocline, South America: 1. Paleomagnetic analysis of Cretaceous and Cenozoic rocks, *J. Geophys. Res.*, *106*, 26,605–26,632.

Lamb, S. (2001b), Vertical axis rotation in the Bolivian orocline, South America: 2. Kinematic and dynamical implications, *J. Geophys. Res.*, *106*, 26,633–26,653.

Libarkin, J. C., R. F. Butler, and D. R. Richards (1998), Tertiary remagnetization of Paleozoic rocks from the Eastern Cordillera and sub-Andean Belt of Bolivia, *J. Geophys. Res.*, *103*, 30,417–30,429.

Loewy, S. L., J. N. Connelly, and I. W. D. Dalziel (2004), An orphaned basement block: The Arequipa-Antofalla Basement of the central Andean margin of South America, *Geol. Soc. Am. Bull.*, *116*, 171–187.

Lyon-Caen, H., P. Molnar, and G. Sùarez (1985), Gravity anomalies and flexure of the Brazilian Shield beneath the Bolivian Andes, *Earth Planet. Sci. Lett.*, *75*, 81–92.

Macedo-Sánchez, O. (1993), Etude paléomagnétique des formations crétacées et tertiaires des Andes Centrales du Pérou. Rôle des rotations dans la formation des déflexions andines, thèse d'université, 298 pp., Univ. Paris XI, Orsay, France.

Macedo-Sánchez, O., J. Surmont, C. Kissel, and C. Laj (1992a), New temporal constraints on the rotation of the Peruvian Central Andes obtained from paleomagnetism, *Geophys. Res. Lett.*, *19*, 1875–1878.

Macedo-Sánchez, O., J. Surmont, C. Kissel, P. Mitouard, and C. Laj (1992b), Late Cainozoic rotation of the Peruvian Western Cordillera and the uplift of the Central Andes, *Tectonophysics*, *205*, 65–77.

MacFadden, B. J., F. Anaya, and C. C. Swisher III (1995), Neogene paleomagnetism and oroclinal bending of the central Andes of Bolivia, *J. Geophys. Res.*, *100*, 8153–8167.

Marocco, R. (1978), Un segment E-W de la chãcirc;ne des Andes péruviennes: La deflexion d'Abancay. Etude géologique de la Cordillère Orientale et des hauts plateaux entre Cuzco et San Miguel, *Trav. Doc. ORSTOM*, 195 pp.

Marocco, R. (1984), Dynamique du remplissage d'un bassin intramontagneux cénozõuml;que andin: Le bassin Moquegua (Sud du Pérou), *Cah. ORSTOM. Sér. Géol.*, *14*, 117–140.

Martignole, J., and J.-E. Martelat (2003), Regional-scale Grenvillian-age UHT metamorphism in the Mollendo-Camana block (basement of the Peruvian Andes), *J. Metamorph. Geol.*, *21*, 99–120.

May, S. R., and R. F. Butler (1985), Paleomagnetism of the Puente Piedra Formation, central Peru, *Earth Planet. Sci. Lett.*, *72*, 205–218.

McQuarrie, N. (2002), Initial plate geometry, shortening variations, and evolution of the Bolivian orocline, *Geology*, *30*, 867–870.

Mégard, F. (1978), *Étude Géologique des Andes du Pérou Central*, 310 pp., INGEOMIN- ORSTOM, Paris.

Mitouard, P., C. Kissel, and C. Laj (1990), Post-Oligocene rotations in southern Ecuador and Northern Peru and the formation of the Huancabamba deflection in the Andean Cordillera, *Earth Planet. Sci. Lett.*, *98*, 329–339.

Mitouard, P., C. Laj, T. Mourier, and C. Kissel (1992), Paleomagnetic study of an arcuate fold belt developed on a marginal orogen: The Cajamarca deflection, northern Peru, *Earth Planet. Sci. Lett.*, *112*, 41–52.

Mukasa, S. N. (1986), Zircon U-Pb ages of super-units in the coastal batholith, Peru: Implications for magmatic and tectonic processes, *Geol. Soc. Am. Bull.*, *97*, 241–254.

Müller, J. P., J. Kley, and V. Jacobshagen (2002), Structure and Cenozoic kinematics of the Eastern Cordillera, southern Bolivia (21°S), *Tectonics*, *21*(5), 1037, doi:10.1029/2001TC001340.

Muñoz, N., and R. Charrier (1996), Uplift of the western border of the Altiplano on a west-vergent thrust system, northern Chile, *J. S. Am. Earth Sci.*, *9*, 171–181.

Noble, D. C., E. H. McKee, T. Mourier, and F. Mégard (1990), Cenozoic stratigraphy, magmatic activity, compressive deformation and uplift in northern Peru, *Geol. Soc. Am. Bull.*, *102*, 1105–1113.

Norabuena, E., L. Leffler-Griffin, A. Mao, T. Dixon, S. Stein, I. S. Sacks, L. Ocola, and M. Ellis (1998), Space geodetic observations of Nazca–South America convergence across the central Andes, *Science*, *279*, 358–362.

Palmer, H. C., A. Hayatsu, and W. D. MacDonald (1980), The middle Jurassic Camaraca Formation, Arica, Chile: Paleomagnetism, K-Ar age dating and tectonic implications, *Geophys. J. R. Astron. Soc.*, *62*, 155–172.

Paquereau, P., J. C. Thouret, G. Wörner, M. Fornari, O. Macedo, and P. Roperch (2005), Caractérisation des ignimbrites néogènes du basin d'Arequipa, *Pérou, C. R. Geosci.*, *337*, 477–486.

Pardo-Casas, F., and P. Molnar (1987), Relative motion of the Nazca (Farallon) and South American plates since late Cretaceous time, *Tectonics*, *6*, 233–248.

Perelló, J., V. Carlotto, A. Zarate, P. Ramos, H. Posso, and A. Caballero (2003), Porphyry-style alteration and mineralization of the middle Eocene to early Oligocene Andahuaylas-Yauri Belt, Cusco Region, Peru, *Econ. Geol.*, *98*, 1575–1605.

Randall, D. E. (1998), A new Jurassic-Recent apparent polar wander path for South America and a review of central Andean tectonic models, *Tectonophysics*, *299*, 49–74.

Randall, D. E., G. K. Taylor, and J. Grocott (1996), Major crustal rotations in the Andean margin: Paleomagnetic results from the Coastal Cordillera of northern Chile, *J. Geophys. Res.*, *101*, 15,783–15,798.

Randall, D. E., A. J. Tomlinson, and G. K. Taylor (2001), Paleomagnetically defined rotations from the Precordillera of northern Chile: Evidence of localized in situ fault-controlled rotations, *Tectonics*, *20*, 235–254.

Renne, P. R., C. C. Swisher, A. L. Deino, D. B. Karner, T. L. Owens, and D. J. DePaolo (1998), Intercalibration of standards, absolute ages and uncertainties in $^{40}Ar/^{39}Ar$ dating, *Chem. Geol.*, *145*, 117–152.

Richards, D. R., R. F. Butler, and T. Sempere (2004), Vertical-axis rotations determined from paleomagnetism of Mesozoic and Cenozoic strata of the Bolivian Andes, *J. Geophys. Res.*, *109*, B07104, doi:10.1029/2004JB002977.

Roeder, D. (1988), Andean-age structure of Eastern Cordillera (Province of La Paz, Bolivia), *Tectonics*, *7, 23–39.*

Roperch, P., and G. Carlier (1992), Paleomagnetism of Mesozoic rocks from the central Andes of southern Peru: Importance of rotations in the development of

the Bolivial Orocline, *J. Geophys. Res.*, *97*, 17,233–17,249.

Roperch, P., G. Herail, and M. Fornari (1999), Magnetostratigraphy of the Miocene Corque basin, Bolivia: Implications for the geodynamic evolution of the Altiplano during the late Tertiary, *J. Geophys. Res.*, *104*, 20,415–20,429.

Roperch, P., M. Fornari, G. Hérail, and G. V. Parraguez (2000), Tectonic rotations within the Bolivian Altiplano: Implications for the geodynamic evolution of the central Andes during the late Tertiary, *J. Geophys. Res.*, *105*, 795–820.

Rousse, S., S. Gilder, D. Farber, B. McNulty, and V. R. Torres (2002), Paleomagnetic evidence for rapid vertical-axis rotation in the Peruvian Cordillera ca. 8 Ma, *Geology*, *30*, 75–78.

Rousse, S., S. Gilder, D. Farber, B. McNulty, P. Patriat, V. Torres, and T. Sempere (2003), Paleomagnetic tracking of mountain building in the Peruvian Andes since 10 Ma, *Tectonics*, *22*(5), 1048, doi:10.1029/2003TC001508.

Rousse, S., S. Gilder, M. Fornari, and T. Sempere (2005), Insight into the Neogene tectonic history of the northern Bolivian Orocline from new paleomagnetic and geochronologic data, *Tectonics*, *24*, TC6007, doi:10.1029/2004TC001760.

Russo, R., and P. G. Silver (1994), Trench-parallel flow beneath the Nazca Plate from seismic anisotropy, *Science*, *263*, 1105–1111.

Scanlan, P. M., and P. Turner (1992), Structural constraints on palaeomagnetic rotations south of the Arica Bend, northern Chile: Implications for the Bolivian Orocline, *Tectonophysics*, *205*, 141–154.

Schmitz, M. (1994), A balanced model of the southern central Andes, *Tectonics*, *13*, 484–492.

Sébrier, M., and P. Soler (1991), Tectonics and magmatism in the Peruvian Andes from Late Oligocene to the present, in *Andean Magmatism and Its Tectonic Setting*, edited by R. S. Harmon and C. W. Rapela, *Spec. Pap. Geol. Soc. Am.*, *265*, 259–279.

Sempere, T., G. Hérail, J. Oller, and M. G. Bonhomme (1990), Late Oligicene–early Miocene major tectonic crisis and related basins in Bolivia, *Geology*, *18*, 946–949.

Sempere, T., G. Carlier, P. Soler, M. Fornari, V. Carlotto, J. Jacay, O. Arispe, D. Neraudeau, and J. Cardenas (2002), Late Permian–Middle Jurassic lithospheric thinning in Peru and Bolivia, and its bearing on Andean-age tectonics, *Tectonophysics*, *345*, 153–181.

Sempere, M., M. Fornari, J. Acosta, A. Flores, J. Jacay, D. Peña, P. Roperch, and E. Taipe (2004), Estratigrafía, geocronología, paleogeografía y paleotectónica de los depósitos de antearco del sur del Perú, paper presented at XII Congreso Peruano de Geología, Soc. Geol. del Perú, Lima.

Sheffels, B. M. (1990), Lower bound on the amount of crustal shortening in the central Bolivian Andes, *Geology*, *18*, 812–815.

Soler, P., and M. Bonhomme (1990), Relation of magmatic activity to plate dynamics in central Peru from Late Cretaceous to present, *Geol. Soc. Am. Bull.*, *241*, 173–192.

Somoza, R. (1998), Updated Nazca (Farallon)–South America relative motions during the last 40 My: Implications for mountains building in the central Andean region, *J. S. Am. Earth Sci.*, *11*, 211–215.

Somoza, R., and A. Tomlinson (2002), Paleomagnetism in the Precordillera of northern Chile (22°30′S): Implications for the history of tectonic rotations in the central Andes, *Earth Planet. Sci. Lett.*, *194*, 369–381.

Somoza, R., S. Singer, and A. Tomlinson (1999), Paleomagnetic study of upper Miocene rocks from northern Chile: Implications for the origin of late Miocene-Recent tectonic rotations in the southern Central Andes, *J. Geophys. Res.*, *104*, 22,923–22,936.

Taylor, G. K., B. Dashwood, and J. Grocott (2005), The central Andean rotation pattern: Evidence of an anomalous terrane in the forearc of northern Chile from paleomagnetic rotations, *Geology*, *33*, 777–780.

Tosdal, R. M., E. Farrar, and A. H. Clark (1981), K-Ar geochronology of the late cenozoic volcanic rocks of the Cordillera Occidental, southernmost Peru, *J. Volcanol. Geotherm. Res.*, *10*, 157–173.

Vicente, J. C. (1989), Early late-Cretaceous overthrusting in the western cordillera of southern Peru, in *Geology of the Andes and Its Relation to Hydrocarbon and Mineral Resources*, *Earth Sci. Ser.*, vol. 11, edited by G. E. Ericksen, M. T. C. Pinochet, and J. A. Reinemund, pp. 91–117, Circum-Pac. Counc. for Energy and Miner. Resour., Houston, Tex.

von Rotz, R., F. Schlunegger, F. Heller, and I. Villa (2005), Assessing the age of relief growth in the Andes of northern Chile: Magneto-polarity chronologies from Neogene continental sections, *Terra Nova*, *17*, 462–471.

Watts, A. B., S. H. Lamb, J. D. Fairhead, and J. F. Dewey (1995), Lithospheric flexure and bending of the central Andes, *Earth Planet. Sci. Lett.*, *134*, 9–21.

Wörner, G., K. Hammerschmidt, F. Henjes-Kunst, J. Jezaun, and H. Wilke (2000), Geochronology (^{40}Ar-^{39}Ar-, K-Ar- and He-exposure ages) of Cenozoic magmatic rocks from Northern Chile (18°–22°S): Implications for magmatism and tectonic evolution of the Central Andes, *Rev. Geol. Chile*, *27*, 205–240.

Wörner, G., D. Uhlig, I. Kohler, and H. Seyfried (2002), Evolution of the West Andean Escarpment at 18°S (N. Chile) during the last 25 Ma: Uplift, erosion and collapse through time, *Tectonophysics*, *345*, 183–198.

Yañez, G., J. Cembrano, M. Pardo, C. Ranero, and D. Selles (2002), The Challenger-Juan Fernandez-Maipo major tectonic transition of the Nazca-Andean subduction system at 33–34°S: Geodynamic evidence and implications, *J. S. Am. Earth Sci.*, *15*, 23–38.

C. Arriagada and C. Tapia, Departamento de Geología, Universidad de Chile, Plaza Ercilla 803, Santiago, Chile.

M. Fornari, IRD, Géosciences Azur, Sophia Antipolis, Parc Valrose, F-06108 Nice cedex 2, France.

M. García, Servicio Nacional de Geología y Minería, av. Santa Maria 0104, Providencia, Santiago, Chile.

C. Laj, LSCE, avenue de la Terrasse, F-91198 Gif-Sur-Yvette cedex, France.

O. Macedo, Instituto Geofisico del Perú, Oficina Regional de Arequipa, Urbanizacion La Marina B-19, Cayma, Arequipa, Peru.

P. Roperch, IRD, UR154 and Géosciences Rennes, Université de Rennes1, Campus de Beaulieu, CS 74205, F-35042 Rennes Cedex, France. (pierrick.roperch@ird.fr)

T. Sempere, IRD, LMTG, avenue Edouard Belin, F-31400 Toulouse, France.